



Computer-aided design of proline-rich antimicrobial peptides based on the chemophysical properties of a peptide isolated from *Olivancillaria hiatula*

Edward Ntim Gasu, John Kenneth Mensah & Lawrence Sheringham Borquaye

To cite this article: Edward Ntim Gasu, John Kenneth Mensah & Lawrence Sheringham Borquaye (2023) Computer-aided design of proline-rich antimicrobial peptides based on the chemophysical properties of a peptide isolated from *Olivancillaria hiatula*, Journal of Biomolecular Structure and Dynamics, 41:17, 8254-8275, DOI: [10.1080/07391102.2022.2131626](https://doi.org/10.1080/07391102.2022.2131626)

To link to this article: <https://doi.org/10.1080/07391102.2022.2131626>



© 2022 The Author(s). Published by Informa UK Limited, trading as Taylor & Francis Group



[View supplementary material](#)



Published online: 11 Oct 2022.



[Submit your article to this journal](#)



Article views: 3059



[View related articles](#)



[View Crossmark data](#)



Citing articles: 6 [View citing articles](#)

Computer-aided design of proline-rich antimicrobial peptides based on the chemophysical properties of a peptide isolated from *Olivancillaria hiatula*

Edward Ntim Gasu^{a,b} , John Kenneth Mensah^a and Lawrence Sheringham Borquaye^{a,b} 

^aDepartment of Chemistry, Kwame Nkrumah University of Science and Technology, Kumasi, Ghana; ^bCentral Laboratory, Kwame Nkrumah University of Science and Technology, Kumasi, Ghana

Communicated by Ramaswamy H. Sarma

ABSTRACT

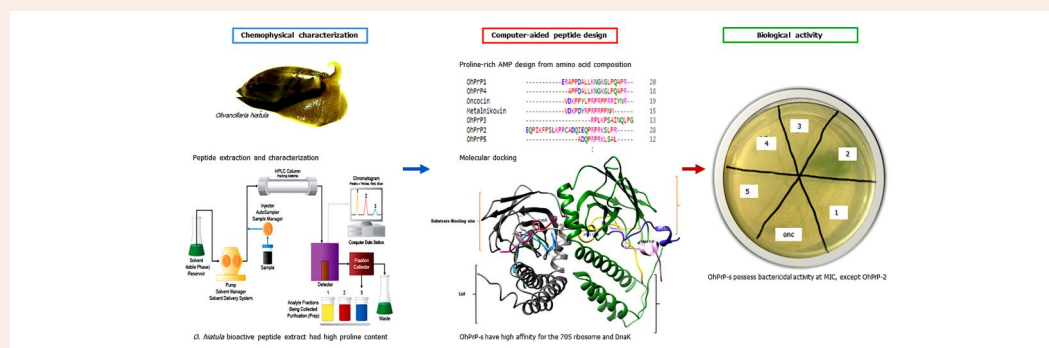
The chemophysical properties of a peptide isolated from *Olivancillaria hiatula* were combined with computational tools to design new antimicrobial peptides (AMPs). The *in silico* peptide design utilized arbitrary sequence shuffling, AMP sequence prediction and alignments such that putative sequences mimicked those of proline-rich AMPs (PrAMPs) and were potentially active against bacteria. Molecular modelling and docking experiments were used to monitor peptide binding to some intracellular targets like bacteria ribosome, DnaK and LasR. Peptide candidates were tested *in vitro* for antibacterial and antiviral activities. Chemophysical studies of peptide extract suggested hydrophobic, acidic and proline-rich peptide properties. The amino acid signature of the extract matched that of AMPs that inhibit intracellular targets. Two of the designed PrAMP peptides (OhPrP-3 and OhPrP-5) had high affinity for the ribosome and DnaK. OhPrP-1, 2 and 4 also had favorable interactions with the biomolecular targets investigated. Peptides had bactericidal activity at the minimum inhibitory concentration against *Pseudomonas aeruginosa*. The designed peptides docked strongly to LasR suggesting possible interference with quorum sensing, and this was corroborated by *in vitro* data where sub-inhibitory doses of all peptides reduced pyocyanin and pyoverdine expression. The designed peptides can be further studied for the development of new anti-infective agents.

ARTICLE HISTORY

Received 30 May 2022
Accepted 27 September 2022

KEYWORDS

Proline-rich AMPs; quorum sensing; peptide docking; pyoverdine; pyocyanin; swarming motility




Introduction

The overuse and misuse of antibiotics in healthcare and agriculture are major factors that have contributed to antimicrobial resistance (AMR). The emergence of multidrug resistance in microorganisms has necessitated a need to develop new antibiotics, preferably with novel targets and modes of action (Beyer & Paulin, 2020; León-Buitimea et al., 2020). Bacteria have the ability to form biofilms and regulate a complicated communication network to control population-dependent behaviors within these biofilms (Kostylev et al.,

2019). Antibiotics are usually very active against planktonic cells but fail with persister cells in biofilms. Compounds that are able to inhibit the viability of planktonic cells and those in biofilms are, therefore, highly desirable.

Antimicrobial peptides (AMPs) are used by many organisms as a first line of defense to kill invading microorganisms (Ganz, 2003), and have been shown to elicit anti-biofilm and anti-quorum sensing effects (Batoni et al., 2016; Pletzer & Hancock, 2016). AMPs are a major constituent of the innate immune system of marine invertebrates. Because marine invertebrates rely on their innate immune system for survival

CONTACT Lawrence Sheringham Borquaye  slborquaye@yahoo.com; lsborquaye.sci@knust.edu.gh  Department of Chemistry, Kwame Nkrumah University of Science and Technology, Kumasi, Ghana

 Supplemental data for this article can be accessed online at <https://doi.org/10.1080/07391102.2022.2131626>

© 2022 The Author(s). Published by Informa UK Limited, trading as Taylor & Francis Group
This is an Open Access article distributed under the terms of the Creative Commons Attribution-NonCommercial-NoDerivatives License (<http://creativecommons.org/licenses/by-nc-nd/4.0/>), which permits non-commercial re-use, distribution, and reproduction in any medium, provided the original work is properly cited, and is not altered, transformed, or built upon in any way.

against pathogenic attack, the AMPs must have evolved to be very effective against these pathogens (Borquaye et al., 2015, 2016, 2017; Destoumieux-Garzón et al., 2016). Marine invertebrates are, therefore, potential sources of AMPs that could be explored for antimicrobial chemotherapy. *Olivancillaria hiatula* is a benthic and sessile marine invertebrate whose interactions with ocean surfaces expose it to numerous biotic pressures including bacterial infections. Adaptation and survival under such conditions make it a potential source of AMPs.

Most AMPs inhibit bacterial growth by permeating the membrane, but other AMPs that target intracellular machineries responsible for bacteria metabolism are also known. Proline-rich AMPs (PrAMPs) belong to a group of cationic AMPs that are enriched in proline residues and are often arranged in conserved patterns together with arginine residues. PrAMPs target key machineries critical for bacteria survival—the ribosome which plays a key role in protein translation and DnaK, a chaperone protein essential in cellular responses to protein unfolding (Genevaux et al., 2004; Jonas et al., 2013). Most antibiotics used clinically block protein synthesis by interacting with the ribosome (Poehlsgaard & Douthwaite, 2005). Thus, inhibiting the ribosome and interrupting the inspection of proper protein folding by inhibiting DnaK, could be an innovative approach in developing antimicrobial agents.

Knowledge of the sequence of AMPs isolated from natural sources is critical in their development as potential drug leads. Primary structure elucidation of isolated AMPs is generally performed using traditional techniques such as reduction and alkylation, amino acid (AA) analysis, proteolytic treatment followed by reverse phase—high performance liquid chromatography (RP-HPLC) purification of peptide fragments, Edman degradation and/or mass spectrometry of the obtained fragments (Sperstad et al., 2011). There are many challenges associated with primary structure elucidation of AMPs isolated in particular, from marine sources. Dimeric peptides, which are a common feature of such AMPs, may generate duplicate intensities during Edman degradation, as was observed for isolation of the centrocins (from the green sea urchin *S. droebachiensis*) (Li et al., 2010), and dicynthaurin and halocidin (from the tunicate *H. aurantium*) (Jang et al., 2002; Lee et al., 2001). These results may be misinterpreted when peptides are impure. Other challenges that may make primary sequence determination difficult include low abundance of peptides from unstimulated animals during peptide isolation, and possible post-translational modifications. To overcome some of these challenges, genome-databases derived from the organisms are mined for the presence of AMPs. To identify potential candidates, computer algorithms are used to derive putative peptides which showed no similarity with already known peptides/proteins and are potentially antimicrobial (Fedders & Leippe, 2008). This strategy for AMP discovery has yielded a number of AMPs (Fedders & Leippe, 2008; Fedders et al., 2008, 2010). Recently, other linear cationic antimicrobial peptides (LCAMPs) have been reported via a *C. intestinalis* genome-wide *in silico* identification program (Ohtsuka & Inagaki,

2020). Such computer-aided approaches which make use of existing experimental data, has enhanced accurate prediction of novel AMPs. Additionally, insight into the mechanisms of action of AMPs, by elucidation of their plausible cellular targets are provided by *in silico* assessments (Matos de Opitz & Sass, 2020; Rončević et al., 2019). This way, probable resistance strategies adopted by pathogens can be predicted and simulated in order to reduce the potential of post-discovery drug resistance (Mant et al., 2019; Wilson et al., 2020).

Limitations in AMP development for clinical application include poor pharmacokinetics, toxicity, inactivation by environmental pH, presence of salts, proteases, plasma proteins or other components. These have to be surmounted to enhance AMP optimization into drugs (Dijksteel et al., 2021). Thus, sequences of bioactive natural peptides may be useful templates for the design of more potent and less toxic versions. A probe into nature's AMP design approaches reveals AA composition, hydrophobic content, net charge and length, as determinants of biological activity, toxicity and biomolecular target interaction (Cruz et al., 2021; Pandit et al., 2021). This work presents the direct use of the AA composition from a bioactive natural peptide (with unknown sequence or genomic data) to design new AMPs with tunable characteristics. Herein, the chemophysical properties—solubility, purity and amino acid composition—of a peptide isolated from *O. hiatula* were analyzed. Afterwards, peptides were designed through arbitrary sequence shuffling, machine learning-assisted AMP prediction and iterative sequence alignments for specific feature recognition. Molecular docking was used to monitor ribosome, DnaK and LasR binding in order to select lead peptides. *In vitro* antibacterial assays were then used to evaluate the outcome of *in silico* experiments for AMP candidate identification.

Materials and methods

Characterization of *O. hiatula* peptide extract

Extraction and solubility tests

Peptide extraction was achieved by soaking of pulverized body tissue of *O. hiatula* in acetic acid (10% v/v). The tissue hydrolysate was obtained by centrifugation followed by ice-cold acetone precipitation and lyophilization (Gasu et al., 2018; Ozols, 1990; Pedersen et al., 1994). Solubility tests in water, 10% (v/v) acetic acid, 25% (v/v) acetonitrile (MeCN) prepared in 0.1% (v/v) trifluoroacetic acid (TFA), 8 M urea, ammonium hydroxide, di-methyl sulfoxide (DMSO) and tween 20, were then assessed. Briefly, approximately 10 mg of the peptide was transferred into polypropylene tubes containing approximately 5 mL of appropriate solvent. Solvent treatment was followed by stirring and sonication. A higher peptide mass was used where peptide was soluble in order to determine what mass of the peptide will lead to the formation of a saturated solution.

UV-Vis analysis and peptide quantification

To determine the wavelength of maximum absorbance of the peptide extract, 1 mg/mL of the extract was prepared in

25% MeCN in 0.1% TFA. A double beam UV–Vis spectrometer and quartz cuvettes (SPECORD 200 PLUS, Model: 223E1451, Analytik Jena, Germany) were used in recording absorption spectrum of the peptide solution in the 190–900 nm range. In the reference cell, 25% MeCN in 0.1% TFA was used. Absorption maxima were determined automatically using default peak picking preferences. Peptides were quantified based on their calculated ϵ_{205} at 1 mg/mL, and their absorbance values at 205 nm and 280 nm (Scopes, 1974). Concentration was determined using Equations (1) and (2):

$$\epsilon_{205}^{1 \text{ mg/mL}} = 27 + 120 \left(\frac{A_{280 \text{ nm}}}{A_{205 \text{ nm}}} \right) \quad (1)$$

$$C = \frac{A_{205 \text{ nm}}}{\epsilon_{205}^{1 \text{ mg/mL}}} \quad (2)$$

Reverse phase-high performance liquid chromatography (RP-HPLC)

Reverse phase-HPLC of the peptide extract was performed on a Cecil Adept Series HPLC system (Cecil Instruments, Cambridge England), fitted with a UV detector. The retention time of the peptide was determined on an analytical reverse-phase Grace Vydac 218TP54 C18 column (300 Å, 5 µm, 4.6 mm i.d. × 250 mm). A gradient of acetonitrile (solvent B) and doubly distilled deionized water (solvent A), from 0% to 70% of B at a flow rate of 1 mL/min for 15 min was used for elution. The gradient elution was run after sample injection and peptides were monitored at 214 nm. Fraction collection was done manually to confirm if the collected peak(s) was the peptide. Elution and manual fraction collection were repeated for scenarios without injection, in order to inspect peptide retention on the column and potential to aggregate in solution. Fractions obtained were dried under nitrogen, reconstituted, re-injected and analyzed under the same conditions as the extract.

AA chromatography

About 20 mg of title peptide extract (labelled I-1) was digested with 6 M HCl at 110 °C for approximately 20 h (Ozols, 1990). AA composition was determined by pre-column derivatization of peptide digest, followed by automated chromatography, as specified in details in the work of Schuster (1988) and Herbert et al. (2000). Two derivatizing agents were simultaneously utilized prior to chromatography of free AAs released into solution after acid digestion of the peptide extract. These were OPA (o-phthalaldehyde) for the primary AAs and FMOC-Cl (9-fluorenylmethylchloroformate) for secondary ones, namely proline and hydroxyproline (Herbert et al., 2000). Norvaline and sarcosine were used as internal standards for the quantification of primary and secondary AAs, respectively. Concentration of free AAs obtained was expressed as percentages and radar-plotted in MS-Excel.

In silico studies

The goal of the *in silico* studies was to provide tentative insights for a well-informed selection of PrAMP candidates for *in vitro* analysis.

Peptide sequence and activity prediction

Since the natural peptide sequence was not successfully determined, a putative peptide sequence; NDDQQQEESSGGRRRAAMILLKKPPPPPP, was propounded from the determined AA composition based on their relative percentages. This sequence was shuffled with the protein shuffle tool of GenScript® Sequence Manipulation Suite (https://www.genscript.com/sms2/shuffle_protein.html) (Stothard, 2000). The shuffles generated were subsequently used to guide prediction and selection of AMPs using CAMP-R3, and later confirmed in DBAASP. Each new random sequence generated from the shuffling suite was added to a list until 160 new algorithmic shuffles were obtained. From this list, a FASTA (Fast-All) file format of the peptide sequences was generated for AMP prediction in CAMPR3 (Collection of Antimicrobial Peptides) (Waghu et al., 2016) using the antimicrobial prediction tool. Prediction criteria were based on peptide length (12–20 AAs), prediction algorithm [artificial neural network (ANN), random forest (RF) and support vector machine (SVM)] and probability of being an AMP (probability score ≥ 0.5). Sequences with high AMP probabilities from CAMPR3, were submitted for AMP prediction confirmation and bacteria-specie specific activity predictions, using the Database for Antimicrobial Activity and Structure of Peptides (DBAASP) (Pirtskhalava et al., 2016). Peptide sequences shown to be active against at least one bacteria specie (positive predictive value (PPV) ≥ 0.5) and inactive towards human erythrocytes were selected.

Peptide sequence alignments and selection

Sequence alignments were carried out to check that putative peptides showed no similarity with already known peptides/proteins but had common features. Every output from DBAASP was subjected to local alignment searches (Basic Local Alignment Search Tool (BLAST)) for the presence of AA motifs such as -LL- and -PR- doublets, as well as -GLP- and -PRP- triplets using CAMPSign (a tool for identification of AMPs using AMP family signatures) (Altschul et al., 1997; Schäffer et al., 2001). Multiple sequence alignment (MSA) in Clustalω (<https://www.ebi.ac.uk/Tools/msa/clustalo/>) (Schäffer et al., 2001) was used to map out common features among generated sequences. Five candidates were finally selected and named as OhPrP-1 to OhPrP-5 (Supporting Information Table S4). OhPrP-2 was designed to defy the stated prediction-selection rules, except that positive predictions in DBAASP alone should be obtained. Hence, OhPrP-2 was obtained from the fusion of a modified OhPrP-5 (-IEQPRPKSLPR-) to arbitrary motifs.

Structure modelling, property predictions and calculations. Peptide structures were modelled using the I-TASSER

(Iterative Threading ASSEmbly Refinement) webserver. Peptide sequences were parsed as FASTA input formats in each server and submitted for structure modelling (Yang & Zhang, 2015). Resulting structural models were written in their PDB formats for molecular docking. Predicted physicochemical properties—Normalized Hydrophobic Moment, Normalized Hydrophobicity, Net Charge, Isoelectric Point, Penetration Depth, Tilt Angle, Propensity to Disorder, Linear Moment, Propensity to *in vitro* Aggregation, Angle Subtended by the Hydrophobic Residues, Amphiphilicity Index and Propensity to PPII coil—were obtained by using the Property Calculation tool in DBAASP. Of these properties, Normalized Hydrophobic Moment, Normalized Hydrophobicity, Linear Moment and Angle Subtended by the Hydrophobic Residues can be calculated by the available hydrophobic scales in DBAASP. Properties of LL-23; (an AMP known to interact strongly with membranes), Oncocin112 and Metalnikowin (known for ribosome and DnaK binding) were predicted as well for comparison purposes and also as a guide to provide insight into potential OhPrP cellular targets. Aggregation propensity was assessed in AGGREGSCAN 3D v2.0 (A3D2) (Kuriata et al., 2019). In A3D2, a dynamic mode was selected in order to include the influence of structural flexibility on protein/peptide aggregation. This allowed server-based default incorporation of the CABS flex protocol.

Molecular docking and visualization

Proline-rich peptides target ribosomes and DnaK to disrupt protein translation and folding, respectively (Gagnon et al., 2016; Roy et al., 2015; Seefeldt et al., 2015). Also, inhibition of ribosomal activity has been highlighted to affect virulence in *Pseudomonas aeruginosa* (Köhler et al., 2007), whereas DnaK inhibition halts swarming motility. Since surface motility is as a result of a quorum response in *P. aeruginosa*, DnaK inhibition may result in disruption of other events (such as inhibition of biofilm formation) controlled by quorum sensing (Okuda et al., 2017). The transcriptional activator, LasR of *P. aeruginosa* is also known to contribute immensely to virulence factor production in quorum sensing. With these in mind, molecular docking to confirm *in silico* antibacterial activity predictions and the validity of the proline-rich AMP propensity of selected AMPs, prior to peptide synthesis and *in vitro* testing, was carried out. LasR was included in molecular docking in order to confirm which target(s) binding and/or inhibition strongly influenced virulence factor expression. Receptors selected were, therefore, the bacterial ribosome, DnaK and LasR, on the premise that peptide binding affinities and interactions could account for potential antibacterial and antivirulence activity in *in vitro* experiments. Peptides (OhPrP-1 to OhPrP-5) were prepared as ligands in each molecular docking experiment. The crystal structures of *Thermus thermophilus* ribosome in complex with Oncocin112 (PDB ID: 4Z8C) (Kuriata et al., 2019), DnaK substrate binding domain of *E. coli* in complex with Oncocin112 (PDB ID: 3QNJ) (Knappe et al., 2011) and LasR-AQS1 complex (PDB ID: 6V7X) (Shah et al., 2021), were accessed from the protein data bank (www.rcsb.org). Ligand–receptor docking was carried out using DINC (for peptides with ≤ 13 AAs) (Antunes et al.,

2017) and HPEPDOCK (Yan et al., 2020) webserver. For docking to the ribosome, the large ribosomal subunit (50S) Chain A was used. For LasR (consisting of the ligand and DNA binding domains) chain B was used and for DnaK, both chains A (DINC) and B (HPEPDOCK) were used. A global receptor search to predict putative peptide-receptor binding modes was made on both servers. Binding affinities were obtained for DINC outputs of OhPrP-3 and -5 only, due to server restrictions on feasible lengths. System visualization and molecular graphics were made in UCSF Chimera (Pettersen et al., 2004) and BIOAVIA Discovery Studio (DS). DS was also used for generation of non-bonding interactions.

In vitro antibacterial and anti-quorum sensing activity

Minimum inhibitory concentration

All five peptides (OhPrP-1 to OhPrP-5) and Oncocin112 were synthesized using the Fmoc method and obtained from Pepmic Co., Ltd (Suzhou, China). Peptides were dissolved in sterile distilled water and 5% (v/v) ACN, and their UV–Vis profiles obtained. Minimum Inhibitory Concentration (MIC) of the peptide extract was determined by the broth microdilution method (Wiegand et al., 2008) against four *P. aeruginosa* strains; ATCC27853, PAO1, PAO1lasB::gfp and a clinical isolate (CI). An inoculum size of approximately 2.0×10^5 CFU/mL of bacteria was added to defined wells of the 96-well plates containing two-fold serial peptide dilutions, and untreated nutrient broth. The plates were then incubated at 37 °C for 24 h. The MIC was determined by visual inspection and absorbance measurements (OD600), as the lowest concentration of peptide that inhibited growth of test organisms.

Minimum bactericidal concentration

The experiment setup used in the MIC determination was repeated. After 24-h of incubation, 10 μ L aliquots from wells containing peptide concentrations greater than and equal to the MIC were plated on sterile agar plates. These were incubated further at 37 °C for 24 h. Minimum bactericidal concentration was recorded as the least peptide concentration that showed no visible bacterial growth.

Growth inhibitory kinetics

The MIC experiment setup was repeated for all bacteria to include absorbance measurements with elapsing time (Campbell, 2011; Vijayakumar & Muriana, 2015). Concentrations tested included the MIC, and sub-MIC concentrations (1/2, 1/4, 1/8, 1/16 and 1/32MIC). Microplates were incubated at 37 °C for an initial 2 h followed by absorbance measurements at 600 nm (OD600) every 30 min for 18 h and the 24th h, with a microplate reader (Synergy H1 multi-mode plate reader, Germany). The OD600 values obtained were plotted against time and used to evaluate the kinetics of bacteria growth at the MIC and sub-MIC concentrations.

Virulence factor inhibition

Inhibition of pyoverdine and pyocyanin expression

P. aeruginosa (PAO1lasB::gfp and clinical isolate) inoculum was incubated in the absence and presence of sub-MIC doses of the peptides at 37 °C for 24 h followed by centrifugation at 4000 rpm for 45 min. One hundred microliters of cell-free supernatant was dispensed into a 96-well microtiter plate for pyoverdine measurement. The relative concentration of pyoverdine (expressed as percentages) in all treated supernatant with respect to control, were measured by fluorescence (BioTek® Synergy H1 multimode microplate reader, Germany) at an excitation wavelength of 405 nm and an emission wavelength of 465 nm (Adonizio et al., 2008; Das et al., 2016).

Similarly, treated and untreated overnight cultures were obtained as described for pyoverdine quantitation experiments. Cell free supernatants were collected after centrifugation at 4000 rpm for 45 min. Pyocyanin extraction was carried out using chloroform. Absorbance of supernatants (pink layer) obtained after acid (0.2 M HCl) treatment of the chloroform extract, was measured at 520 nm (Musthafa et al., 2012). Pyocyanin concentration (µg/mL) was calculated by multiplying the absorbance value at 520 nm with 17.072 (molar extinction co-efficient of pyocyanin at 520 nm) and expressed as percentages.

Swarming motility assay

Swarming motility was analyzed in cultures of *P. aeruginosa* (PAO1, lasB::gfp and clinical isolate) using a swarming motility agar (0.8% nutrient broth, 0.5% nutrient agar and 0.5% glucose). The media surface was briefly dried, and a single colony inoculated using a sterile toothpick at the center of the agar surface and incubated at 37 °C for 12 h and 24 h. The diameter of the featherless mat was measured accordingly (Inoue et al., 2008).

Results

Characteristics of *O. hiatula* peptide extract

Tissue hydrolysate (extract) obtained by addition of 10% glacial acetic acid, followed by centrifugation had a characteristic tan to cream color. Extraction yields after precipitation and freeze-drying were 25.4% and 3.0%, respectively, relative to tissue mass. The peptide extract was soluble in 25% ACN prepared in 0.1% TFA and ammonium hydroxide, with foaming upon shaking (Supporting Information Table S1). The absorption of UV-Vis radiation by peptide bonds, aromatic side chain and other chromophores was evaluated for qualitative and quantitative purposes. The maximum absorbance of the peptide solution (1.08 A) occurred at 194 nm, with a smaller shoulder at 240 nm (0.22 A), and a weaker band at 280 nm (Figure 1). The extinction co-efficient ($\epsilon_{205\text{ nm}}^{1\text{ mg/mL}}$) was calculated to be 31.013 mL.mg⁻¹cm⁻¹ using Scope's method, and this led to an estimated concentration of 0.207 mg of protein/mL (Supporting Information Table S2).

The purity of the peptides was evaluated by RP-HPLC. A single peak at 5.45 min was observed (Figure 2). The concentration of ACN present at the elution time of the peptide was between 55 and 60% (Supporting Information Figure S1). A good overlap of peak shape and retention time match of re-injected fraction was observed, and this was comparable to main peptide chromatogram. Inconsistent overlap of peaks was observed for solvent used for reconstitution of dried fraction (Supporting Information Figure S1c; A and B). Re-run of gradient elution without new injections led to the elution of peptide molecules retained on the column (Supporting Information Figures S1b (A and B), even for re-injected fractions (Supporting Information Figure S1c; B).

Analysis of the AAs in the peptide was used for molecular characterization (Huan et al., 2020; Mishra & Wang, 2012; Ozols, 1990). The peptide was subjected to strong acid digestion before AA compositional analyses were done. The aspartic acid concentration (Asp + Asn) was found to be 282.16 pmol/µL, whereas glutamic acid concentration (Glu + Gln) was 608.47 pmol/µL (Supporting Information Table S3). Percentage estimates (Figure 3) of all 15 AAs detected revealed little aromatic contribution. Proline was considerably the highest AA constituent of the peptide. Alanine, glutamic acid, aspartic acid, leucine, glycine, arginine and lysine were present at moderate levels. Valine was the least, while phenylalanine was the only aromatic AA detected.

In silico studies

Peptide sequence and activity prediction

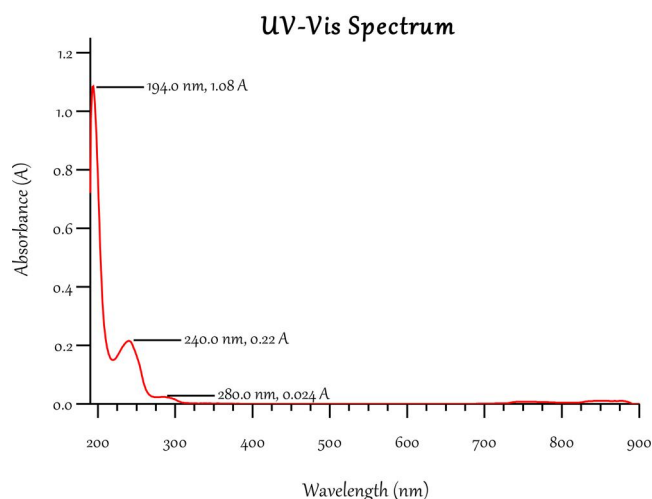
About 160 sequences were generated from sequence shuffling and multiple sequence alignments for the shuffled sequences (sections shown as Supporting Information Figure S2a). OhPrP-4 differed very little from OhPrP-1 by just two AAs, whereas OhPrP-3 and OhPrP-5 shared some segments in common with OhPrP-2 (Supporting Information Figure S2c). AMP-like sequence prediction by length, machine learning algorithm and predictive probability in CAMPR3, from selected shuffles, gave approximately 380 sequences predicted as AMPs. Their predictive probabilities ranged from 0.486 to 0.938. The ANN prediction algorithm gave the highest AMP-like sequences generated (269 of all 380), followed by the SVM and RF algorithms. Sixty-five of these sequences were confirmed to be AMP-like in DBAASP.

Of these 65 sequences, 27 (Supporting Information Figure S2b, A) emerged from ANN predicted outcome (prefixed by seq_ANN in the figure) as possibly active against designated bacteria species. Each putative sequence was shown to probably inhibit either *K. pneumoniae*, *E. coli* ATCC 25922 or *B. subtilis*. Overall, five putative sequences were chosen, namely OhPrP-1, -3, -4 and -5, with OhPrP2 designed as described earlier to be a negative control. Specifically, OhPrP-1, 3 and 4 were predicted to possess antibacterial activity against *B. subtilis*; with a common positive prediction value (PPV) of 0.81. OhPrP-1 and OhPrP-5 with PPVs of 0.85 and 0.90, respectively, were projected as possible *K. pneumoniae* inhibitors. OhPrP-2 was predicted to be active against *B. subtilis*.

Table 1. Amino acid sequences of candidate peptides based on putative peptide sequence shuffling and database predictions, retention time, percentage purity and quantity of synthetic oligomers obtained.

Peptide	Sequence	Retention time (min)	Purity (%)	Quantity (mg)
OhPrP-1	ERAPDALLKNGKGLPQAPR	8.93	74.45	200
OhPrP-2	EQPIKFPSPKPRCADQIEQPRPKSLPR	9.10	73.66	200
OhPrP-3	RPLKPSAINQLPG	9.04	61.09	200
OhPrP-4	APPDALLKNGKGLPQAPR	9.50	79.72	200
OhPrP-5	ADQPRPKLSAL	8.20	75.47	200
Oncocin112	VDKPPYLP RP RP RR IYNR	8.87	69.01	200
LL-23+	LLGDFFRKSKEKIGKEFKRIVQR	9.702	96.27	N/A

+: Retention and sequence of a membrane targeting AMP (LL-23) Adapted from the work of Mishra and Wang (2012).

**Figure 1.** Ultraviolet-visible wavelength of absorption spectrum of peptide extract using ultraviolet-visible spectroscopy. Maximum absorbance (1.08 Å) occurred at 194 nm and a lower shoulder at 240 nm (0.22 Å), due to peptide backbone ($\pi \rightarrow \pi^*$ transitions) and contributions from side chains of aspartic acid (Asp), glutamic acid (Glu), asparagine (Asn), glutamine (Gln), arginine (Arg) and/or histidine (His). The weakest absorption was observed at 280 nm, due to aromatic amino acids (AA).

(0.81), *P. aeruginosa* ATCC 27583 (0.62) and *E. coli* ATCC 25922 (0.58). Predictions for Oncocin112 show potential activity against *K. pneumoniae* (0.85), *E. coli* ATCC 25922 (0.59), *P. aeruginosa* ATCC 27583 (0.65) and *S. aureus* (0.57). All peptides, including Oncocin112, were predicted to be inactive against human erythrocytes. Following these outcomes, the five peptide sequences (Table 1; OhPrP-1 to OhPrP-5) were earmarked for molecular docking.

Structure modelling and property calculations

The I-TASSER server matched the predicted 3D models to the proteins in independent libraries, as part of its default mode of operation. Models were ranked based on the confidence score of the I-TASSER structural models, the structural similarity between model and templates and the sequence identity in the structurally aligned regions. Afterwards, a final set of output structures are reported in PDB formats. For OhPrP-1, -2, -3 and -4, a coil-helix-coil structure was predicted. In contrast, a predominantly coiled structure for OhPrP-5 and Oncocin112 was predicted (Figure 4(a)). Sequence of segments responsible for helical structures were -PDALLK-, -RCADQI-, -PSAIN- and -PDALLK-, for OhPrP-1, 2, 3 and 4, respectively. OhPrP-1 and OhPrP-4 had very similar sequences; hence, structural similarity was observed. OhPrP-2 and OhPrP-3 were symmetrical.

Interestingly, threading templates used by I-TASSER to build peptide models were related to the ribosomal protein entities and those acting nucleic acids. Notable instances observed were for both OhPrP-1 and 4, where both matched well with a ribonucleoprotein of *T. thermophilus* ribosome (PDB: 4ZSN; Entity 21:Q5SIH3). Also, OhPrP-2 had good structural coverage with *Trypanosoma brucei* ribosomal protein entity 5 (PDB ID: 4V8M, Entity 5: Q38FD9). OhPrP-3 was structurally similar to the structure of the spliceosomal protein p14 segment (PDB ID: 2F9J), and Chain C of the Transposon Tn7 transposition protein tnsC (PDB ID: 1T0F; P05846). OhPrP-5 also, matched with Metalnikowin and Api137 (both being PrAMPs) in complex with *T. thermophilus* ribosome, under the PDB accession codes 5HCP and 5O2R, respectively (Figure 4(b)).

Root-mean-square fluctuations (RMSF) calculated in CABS flex (Supporting Information Figure S3) showed high residue fluctuations within coiled segments of all peptide structures, except regions forming alpha-helices. Normalized beta factors scaled from 0 to 2, with the highest values for loop-like structures from the N-termini towards the center and away towards the C-termini in each structure. Also, RMSF of OhPrP-5 decreased from the N-termini towards Arg7 (mid-way) and increased gradually through to the C-terminus (Supporting Information Figure S3). All peptides were predicted to be water soluble proteins following predictions from the AGGRESCAN 3D webserver. In effect, all predictions suggested enhanced hydrophilic properties as shown by hydrophobicity surfaces (Figure 5).

Since the sequence of the PrAMP—Metalnikowin—was identical to that of Oncocin112 (Supporting Information Figure S2b, B) and was also a match for OhPrP5, its properties were evaluated *in silico* as well. LL-23 is a well-known membrane targeting AMP, and was, therefore, used as a template to provide insights to validate probable targets of the designed peptides. From the estimates of the Moon–Fleming (MN) scale, all the peptides had a net charge of +2, except for OhPrP-2, Oncocin112 and LL-23, which had a charge of +4, +5 and +5, respectively (Table 2). All peptides including Oncocin112 had no propensity to aggregate *in vitro*, following a zero (0) score prediction from DBAASP. Amphiphilicity indices ranged from 0.57 (OhPrP-3) to 0.97 (OhPrP-2) for the designed peptides, but 1.37 and 1.07 for Oncocin112 and Metalnikowin, respectively. Also, peptides had high propensities to coil, with lipid membrane penetration depths of 30, except OhPrP5 (21) and LL-23 (27). Isoelectric points estimated were similar for all peptides, ranging from 10.30 to 11.60. OhPrP-5 recorded the highest tilt angle (160), followed

Table 2. Overview of properties of designed peptides compared to Oncocin112 and Metalnikowin.

ID	Normalized hydrophobic moment	Normalized hydrophobicity	Net charge	Isoelectric point	Penetration depth	Tilt angle	Disordered conformation propensity	Linear moment	Propensity to <i>in vitro</i> aggregation	Angle subtended by the hydrophobic residues	Amphiphilicity index	Propensity to PP11 coil
OhPrP-1	1.12	-0.50	2.00	10.67	30	91	-0.19	0.34	0.00	60.00	0.74	1.11
OhPrP-2	0.32	-0.41	4.00	10.86	30	95	-0.32	0.16	0.00	40.00	0.97	1.24
OhPrP-3	0.13	-0.84	2.00	11.38	30	109	-0.09	0.20	0.00	100.00	0.57	1.21
OhPrP-4	1.19	-0.68	2.00	10.71	30	91	-0.10	0.38	0.00	80.00	0.61	1.14
OhPrP-5	0.33	-0.40	2.00	11.23	21	160	-0.25	0.36	0.00	60.00	0.82	1.17
Oncocin112	0.52	-0.78	5.00	11.59	30	145	-0.56	0.31	0.00	80.00	1.37	1.38
Metalnikowin-1	0.64	-0.52	2.00	10.50	30	69	-0.53	0.21	0.00	100.00	1.07	1.40
LL-23	1.20	0.11	5.00	11.14	27	27	-0.24	0.34	0.00	80.00	1.28	0.90

by Oncocin112 (145) and OhPrP-3 (109). OhPrP-2, and 1, 4, had tilt angles of 95 and 91, respectively (Table 2). The angles subtended by hydrophobic residues as predicted in DBAASP, matched well with CAB-flex modelled hydrophobic surfaces (Table 2 and Figure 5) obtained. Both revealed the least angle for OhPrP-2 (40) and the highest for OhPrP-3 (100).

Variations in physicochemical properties (hydrophobic moment, hydrophobicity, linear moment and angles subtended by hydrophobic residues) were generally observed for all peptides among the different scales. However, for LL-23, only the hydrophobic moment, hydrophobicity and linear moment varied among all the six scales (Supporting Information Table S5). The RP-HPLC retention times for oncocin112 and LL-23 were 8.87 min and 9.702 min, respectively. On the MN scale, angle subtended by hydrophobic residues of both LL-23 and Oncocin112 w 80.00, with linear moments of 0.34 and 0.31, respectively. Depths of penetration for LL-23 and oncocin112 were in close range; however, there was a huge variation in tilt angles (27 and 145, respectively). Similarly, OhPrP1 and OhPrP4 had retention times of 8.93 min and 9.50 min, respectively. The angle subtended by their hydrophobic residues were 60 and 80, respectively, but tilt angles and lipid membrane penetration depths were the same (91 and 30). OhPrP-5 had the least lipid membrane penetration depth in all, but with a tilt angle of 160 and hydrophobic residues subtended at an angle of 60 as OhPrP-1, the retention time obtained was 8.2 min. OhPrP-3 had a retention time of 9.04 min compared to OhPrP-5 which had a retention time of 8.2 min. Tilt angles were similar, however, lipid penetration depths and angles subtended by their hydrophobic residues varied markedly, accounting for differences in their retention times. Also, OhPrP-2 had the highest amphiphilicity index closest to LL-23 and oncocin112, lipid penetration depth of 30, accounting for a retention time of 9.10 min. Overall, though hydrophobicity and hydrophobic moment are crucial for peptide interaction with lipid membranes, in this case the material of the RP-HPLC column used, it was seen that linear moment, angle subtended by hydrophobic residues, number of hydrophobic residues, lipid membrane penetration depths and tilt angles, taken together, greatly influenced the recorded column retention times obtained.

Predicted target binding modes and interactions

A global search of how the peptide constructs interacted with selected cellular targets using molecular docking was implemented. The DINC webserver predicted both binding conformation and binding affinity of peptides with ≤ 13 AAs, whereas HPEPDOCK produced favorable binding modes for all peptides. The full length Oncocin112 has 19 AAs (AA) whereas co-crystallized versions had 13 AAs in both ribosomal and DnaK complexes. Visual inspection together with estimated binding affinities was useful for selection of favorable peptide binding modes. Re-docking of the native peptide fragment of Oncocin112 found in complex with *T. thermophilus* ribosome (PDB ID: 4Z8C), gave a binding pose at the A-site, similar to the crystallized conformation. The

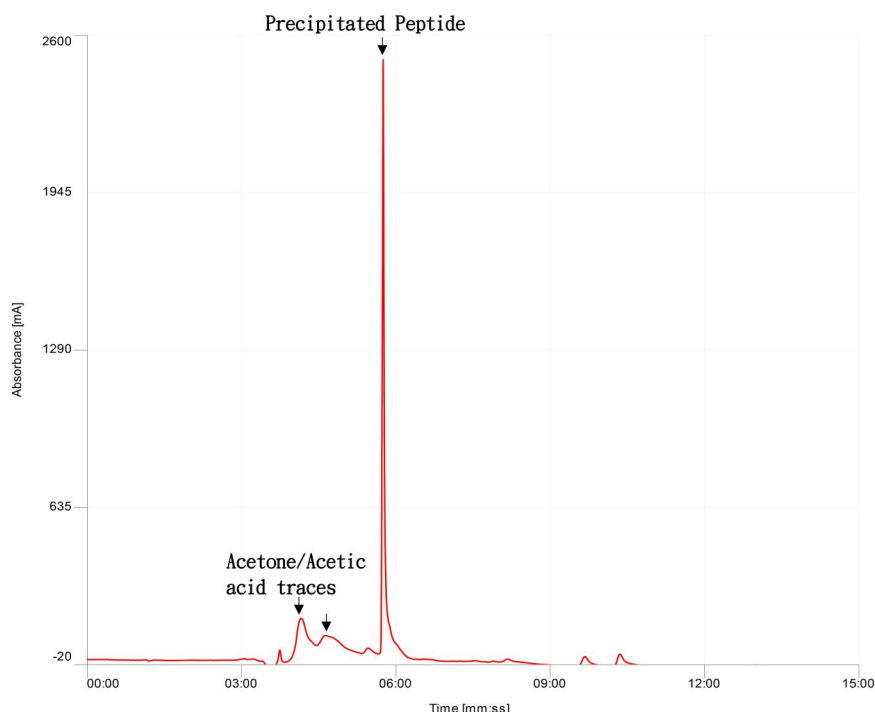


Figure 2. RP-HPLC profile of peptide extract. The retention time of the peptide (most intense peak 1) was measured on a Cecil Adept Series HPLC system equipped with an analytical reverse-phase Vydac 218TP54 C18 column (300 Å, 5 µm, 4.6 mm i.d. × 250 mm) and a UV detector. The peptide detected at 214 nm (retention time: 5:45.8 mm:ss) was eluted with a gradient of acetonitrile, from 0% to 70% at a flow rate of 1 mL/min. Background noise (retention ≤5:00 and >9:00 min:ss) resulted from traces of acetone/acetic acid.

Table 3. Minimum inhibitory concentrations (MIC) of peptide oligomers against *Pseudomonas aeruginosa*.

Peptides	MIC (mM) of <i>Pseudomonas aeruginosa</i> strains			
	ATCC27853	PAO1	PAO1::gfp	Clinical isolate (CI)
Oncocin112	0.24			
OhPrP-1	0.32			
OhPrP-2	0.17			
OhPrP-3	0.31			
OhPrP-4	0.35			
OhPrP-5	0.46			

predicted binding pose aligned well with the experimentally determined conformation (RMSD = 4.59 Å) with a binding affinity of -10.10 kcal/mol. In both conformers, side chain residues of the central core (– 5PYLPRP10 –) aligned well within the A-site crevice region of the ribosome, in contrast to the predicted conformer obtained from the HPEPDOCK (Figure 6(a)). From the superimposition it was observed that, Tyr6 of the HPEPDOCK conformer, stacked with Pro5 of the experimental structure, showing a distortion in the peptide backbone conformation. This distortion resulted in the recorded shift of about 4.03 Å between atoms of the respective proline residues (Figure 6(a)). The full length Oncocin112 binding conformation predicted from the HPEPDOCK web-server, aligned well upon superimposition with the native Oncocin112 structure, however, with an inverted orientation and flanking N- and C- termini segments (Supporting Information Figure S4; A). Peptide backbones of Metalnikowin and Oncocin112 matched well, with little deviations resulting from varying residues (Figure 6(b)).

The designed peptides were also accommodated in the active sites of the ribosome. OhPrP-3 and OhPrP-5 were predicted to bind at the A-site with binding affinities of -9.00

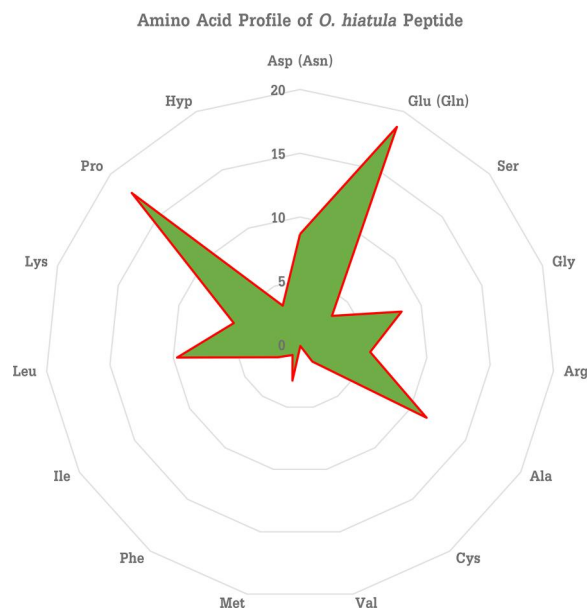


Figure 3. Radar plot showing percentage AA composition of peptide extract. Asp(Asn) represents the percentage of aspartic acid and the contribution of asparagine, as well, Glu(Gln) glutamic acid and corresponding glutamine composition. Hyp represents hydroxyproline whiles all remaining AAs are represented by their standard 3-letter codes.

and -9.30 kcal/mol, respectively. Though bound within the same site as Metalnikowin, OhPrP-3 binds to the CCA-binding site through its N-terminus region, with the C-terminus deviating slightly from the peptidyl-transferase center (PTC) towards the ribosomal exit tunnel. On the contrary, OhPrP-5 binds with an inverted stereo conformation starting with its C-terminus binding to the CCA-binding site and its N-terminus towards the PTC. The C-terminus and N-terminus of

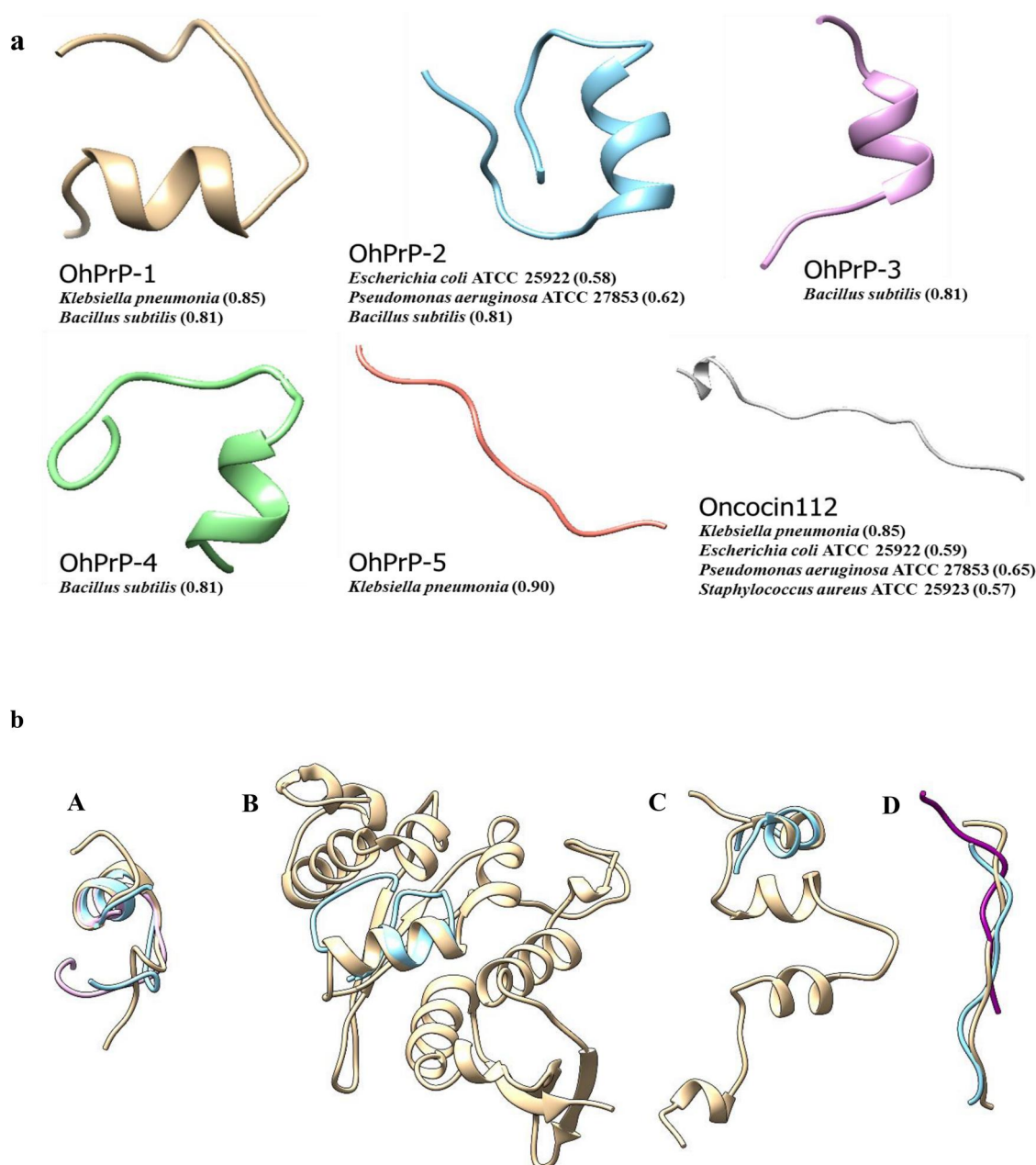


Figure 4. (a) Three dimensional structures of designed peptides obtained from I-TASSER showing DBAASP prediction of specie specific activity. Probabilistic positive predictive value (PPV) have been provided for each peptide. (b) Three dimensional structures of designed peptides obtained from I-TASSER aligned unto their threading templates. (A) OhPrP-1 (sky blue), OhPrP-4 (purple) and *T. thermophilus* ribosome (PDB: 4ZSN) Entity 21:Q5SIH3 (tan). (B) OhPrP-2 (sky blue) and *Trypanosoma brucei* ribosomal protein entity 5 (PDB ID: 4V8M, Entity 5: Q38FD9) (tan). (C) OhPrP-3 and Chain C of the Transposon Tn7 transposition protein tnsC (PDB ID: 1T0F; P05846) (tan). (D) Metalnikowin (dark magenta, PDB ID: 5HCP, chain X), Apidaecin (tan, PDB ID: 5O2R, chain Z), OhPrP-5 (sky blue).

OhPrP-3 and OhPrP-5, respectively, flanked Oncocin112 (Figure 6(b)). Both OhPrP-1 and OhPrP-4 had binding poses spanning the PTC and the upper ribosomal exit tunnel, unlike OhPrP-2 which binds to the exit tunnel (Figure 7).

The binding of Oncocin112 to DnaK was reproduced when the DINC webserver was used. A binding affinity of -7.70 kcal/mol and an RMSD of 3.42 Å relative to the input experimental conformation was recorded (Figure 8). Binding pose of the full length Oncocin112 predicted from the HPEPDOCK server, also matched with the experimental conformer (Supporting Information Figure S4; B) with excellent conserved central core alignment. OhPrP-3 and OhPrP-5

were bound in the DnaK substrate binding site with binding affinities of -7.30 and -7.10 kcal/mol, respectively (Figure 9). The positions of OhPrP-3 and OhPrP-5 were similar to the positions of Oncocin112. OhPrP-1 and 4 were also bound with sterically favored coiled portions to the substrate binding site. An alpha helical fold introduced a symmetrical conformation in the binding pose of OhPrP-2, such that it is binding to the substrate binding domain was achieved through the loop formed from Glu1 to Arg12. Both the helical fold and the loop of the second half of the OhPrP-2 conformer extended into the periphery of the DnaK substrate binding pocket (Figure 9).

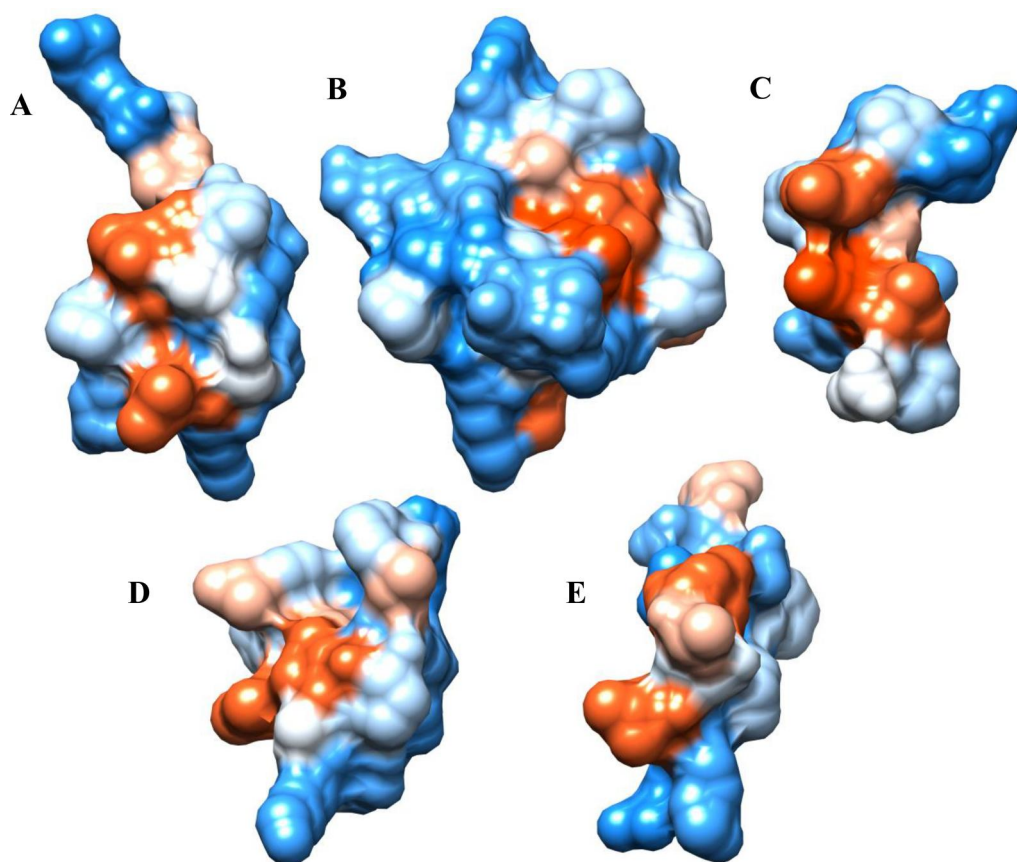


Figure 5. AGGRESCAN 3 D predicted surface exposure to solvent after solubility/aggregation predictions and CABS flex simulation. Output structures were used to generate hydrophobicity surface of peptides (A to E: OhPrP- 1 to 5). Surface coloring; shades of blue to shades of red, depict increasing hydrophobicity.

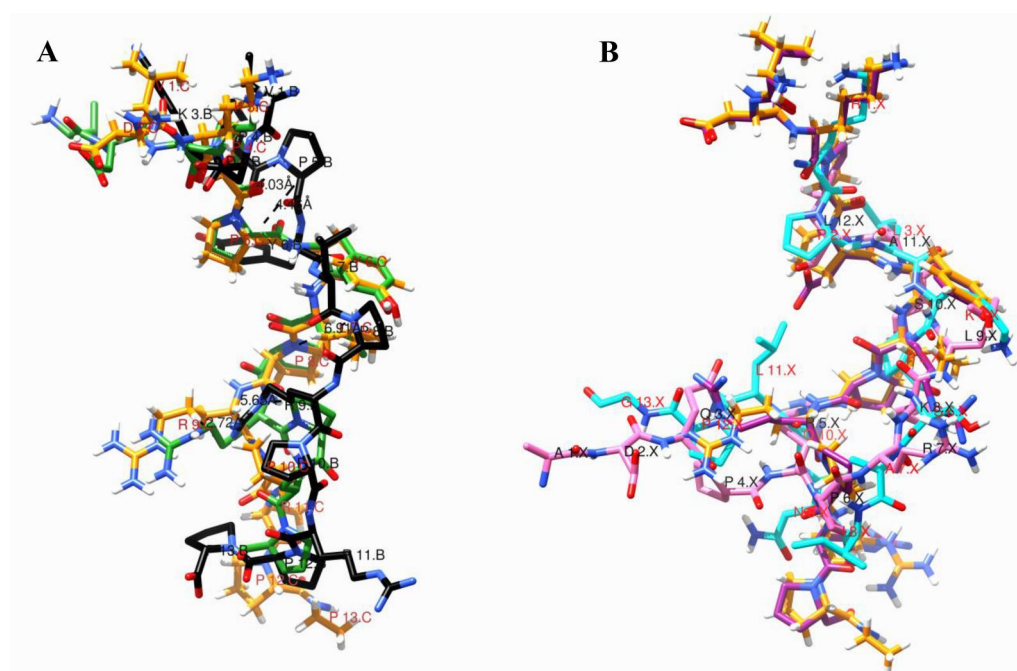


Figure 6. Putative binding modes obtained from molecular docking of peptides to *Thermus thermophilus* ribosome (PDB ID: 4Z8C; 50S subunit). (A) Comparison of the predicted binding modes of Oncocin112 using the DINC webserver (-10.10 kcal/mol; green carbon atoms) and HPEPDOCK (black carbon atoms), to native Oncocin112 binding mode (orange carbon atoms). HPEPDOCK prediction of Oncocin112 binding deviated significantly compared to that of the pose obtained from the DINC webserver which overlapped with the common core of experimental pose. Output binding coordinates of OhPrP-3 (-9.00 kcal/mol) and OhPrP-5 (-9.30 kcal/mol) predicted from DINC depicts binding at the same site as Metalnikowin and Oncocin112: (B) superposition of Metalnikowin (dark magenta), OhPrP-3 (cyan), OhPrP-5 (pink) on Oncocin112 (orange).

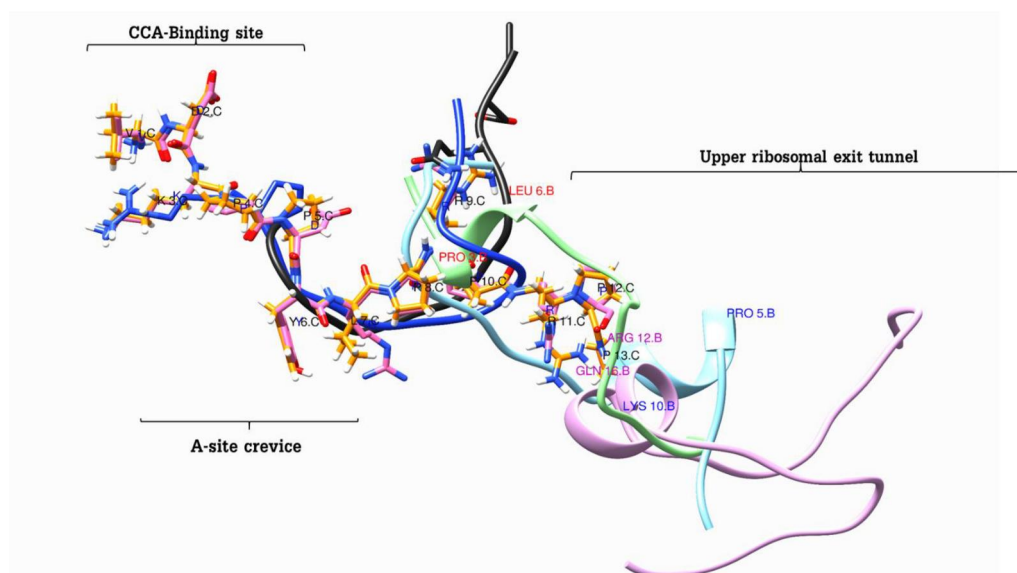


Figure 7. Predicted binding modes of OhPrP-1 (sky blue), OhPrP-2 (orchid) and OhPrP-4 (green) compared to native binding coordinates of Oncocin112 (orange carbon atoms) and Metalnikowin (pink carbon atoms) in the 50S subunit of the *Thermus thermophilus* ribosome (PDB ID: 4Z8C). Blue and black ribbons represent OhPrP-3 and OhPrP-5, respectively. NB: Tube models apply for Oncocin112 and Metalnikowin only, whereas OhPrPs were represented as ribbon models.

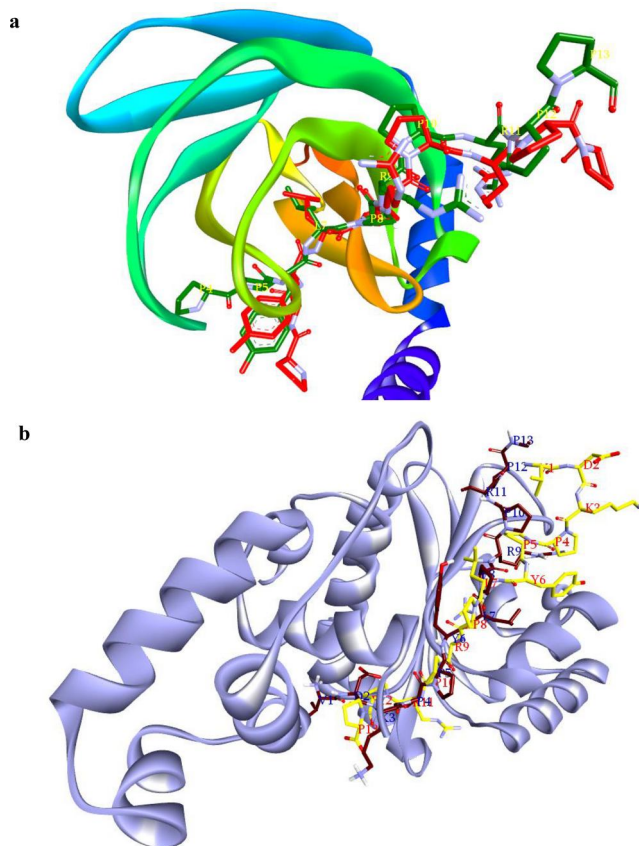


Figure 8. (a) Comparison of predicted binding mode of Oncocin112 co-crystallized with DnaK (PDB ID: 3QNJ) using DINC (red) to experimental conformer. Binding energy for Oncocin112 conformation deviating 3.42 Å from the input conformation was -7.7 kcal/mol. (b) Comparing predicted binding pose of Oncocin112 to LasR, from DINC (red) and HPEPDOCK (yellow). Single letter AA residue labels and identifiers included to show stereo reversion modes of predicted binding conformations.

Both the full length and the 13-mer Oncocin112 structures docked well to the LasR SLR, with less conserved segment alignment, observed from inspection of binding modes

(Supporting Information Figure S4; C). The binding affinity estimated was -8.10 kcal/mol. Also, a prediction of the binding mode of Oncocin112 versus LasR, using HPEPDOCK, produced a similar binding mode as that obtained using DINC, with inverted stereo conformation and flanking of terminal peptide segments (Figure 8b). Comparatively, OhPrP-3 and OhPrP-5 were bound at the SLR-binding domain with binding affinities of -6.90 and -6.20 kcal/mol, respectively. Interestingly, OhPrP-1 and OhPrP-2, preferred the LasR DNA binding domain, whereas OhPrP-4 preferred the loop region of the SLR site (Figure 10(b)). Peptides strongly interacted with major active site residues of the 16S and 23S rRNA, the substrate binding sites of DnaK and the LasR SLR- and DNA- binding domains. Non-bonding interactions are presented as Supporting Information generated from Figures S5a–S7f and Tables S6–S11.

In vitro antibacterial and anti-quorum sensing activity

Antimicrobial activity

The broth microdilution method was used to assess the antibacterial activity of the designed peptides. During preparation, OhPrP-1, –3 and –5 had slight turbidities when dissolved in water, while Oncocin112, OhPrP-2 and –4 were completely soluble in water. UV–Vis spectral scan produced an absorption maximum at 194 nm for all peptides. Only, Oncocin-112 had extra absorptions at 220 nm and 280 nm (Supporting Information Figure S8). The same concentration of each designed peptide was required to inhibit growth of the different *P. aeruginosa* strains used (Table 3). OhPrP-2 had an MIC of 0.17 mM, however, this concentration was found to produce a bacteriostatic effect after re-incubation on agar for another 24 h (Figure 11). The remaining peptides produced bactericidal activity at their MICs (Table 3). Oncocin112 prolonged the lag times of bacterial growth at half-MIC concentration (Figure 12). This was similar for

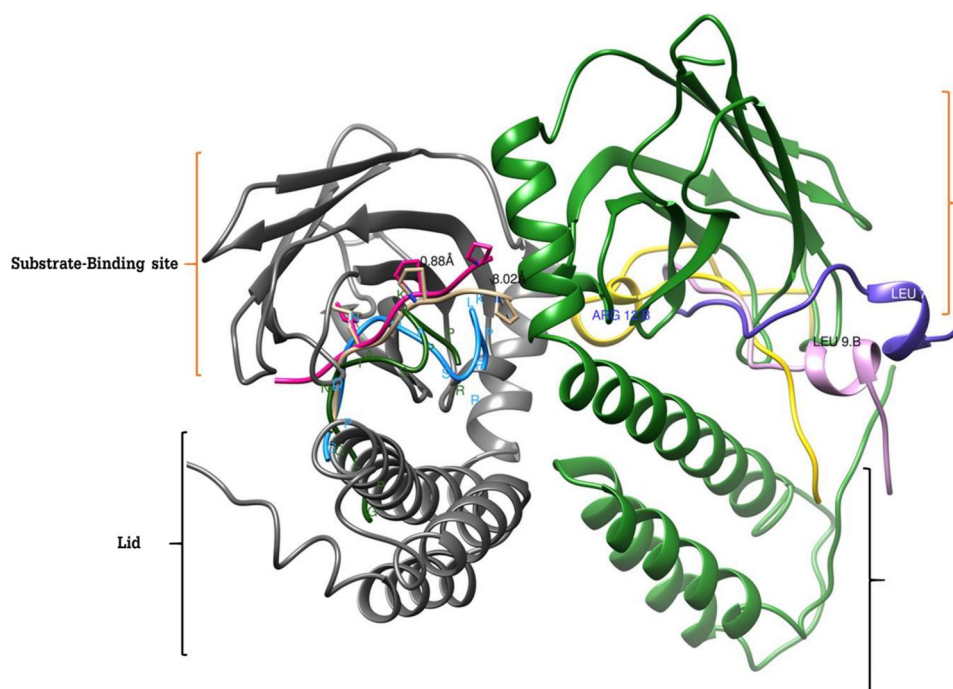


Figure 9. Binding modes of OhPrP-1 to 5, predicted using the DnaK receptor; with ribbons colored black and green (PDB ID: 3QNJ). Tan and magenta ribbons represent experimental and predicted binding poses, respectively, of Oncocin112. Blue and forest green ribbons in the grey DnaK chain represent binding modes of OhPrP-3 and 5, respectively. Binding poses of OhPrP-1, 2 and 4; pink, yellow and purple, relative (single residue labels included to show coiled regions) to green DnaK chain.

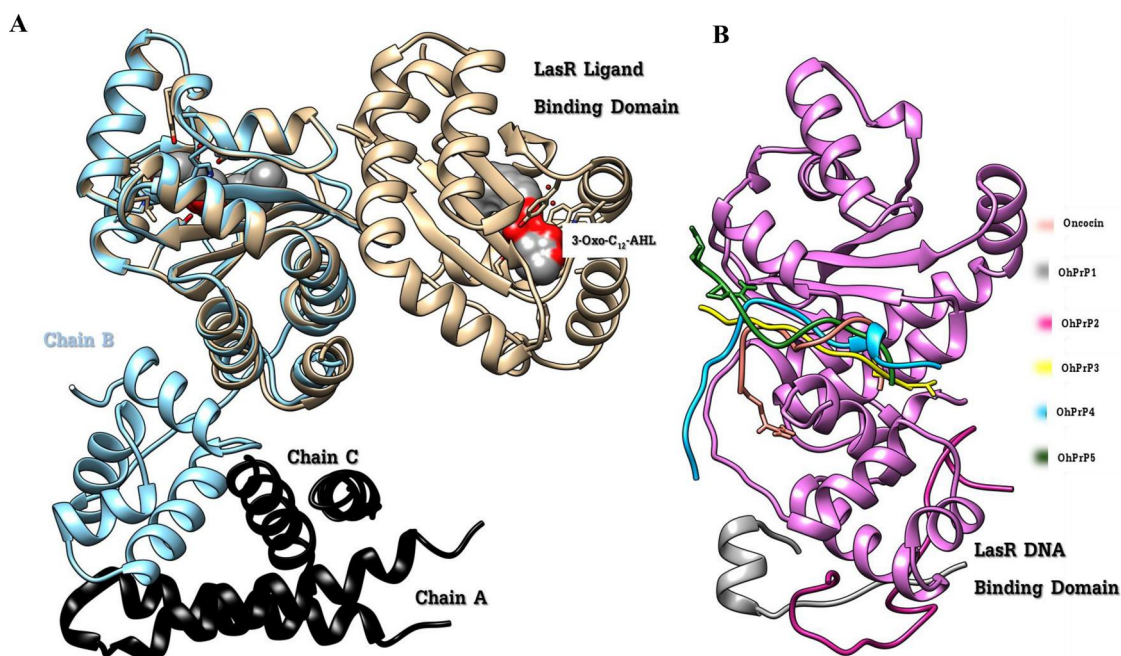


Figure 10. Illustration of (A) *P. aeruginosa* lasR transcriptional activator protein (PDB ID: 2UV0, Chain B; color) in complex with AQS1 (Chain A and C; black), crystal structure of ligand binding domains (tan) given by the PDB accession code 3IX3 (co-crystallized with its autoinducer 3-Oxo-C12-AHL) and (B) binding modes of Oncocin112 and OhPrP-1, 2, 3, 4, 5 (color coded legend to the right).

OhPrP-3 (Figure 15) than for OhPrP-5 (Figure 17) treated cultures. Growth in bacteria cultures containing sub-MIC concentrations of OhPrP-1 to 5, gave higher turbidities compared to the growth control. OD600 recorded at MIC remained mostly constant throughout the incubation period for all bacterial strains tested (Figures 12–17).

Anti-quorum sensing activity

The ability of peptides to interfere with quorum sensing was measured through pyocyanin quantitation, pyoverdine fluorescence measurement and swarming capacity at sub-inhibitory concentrations. The extent of pyocyanin inhibition was generally not dose dependent in all cases, but there was a general

decrease from MIC/2 to MIC/32. While the pyocyanin inhibitory effect of OhPrP-4 remained fairly constant (78%) at all sub-inhibitory concentrations for the PAO1-lasB::gfp strain (Figure 18(a,c)), a dose dependent effect (71.64%; MIC/2, 12.71%; MIC/32) was observed for the clinical isolate. Oncocin112, OhPrP-1



Figure 11. Determination of bacterial killing concentration. MIC gave bactericidal effect at the end of the second half of incubation of plated cultures on agar for; (1) OhPrP-1, (3) OhPrP-3, (4) OhPrP-4, (5) OhPrP-5 and ('onc') Oncocin112. (2) OhPrP-2 inhibited bacterial growth for about 40 h (broth dilution method incubation time inclusive), after which growth (green pyocyanin patch) was observed on the surface of agar.

and 3, inhibited pyocyanin levels expressed similarly in both the PAO1-lasB::gfp strain and the clinical strain. In general, OhPrP-5 produced the least pyocyanin inhibitory effect. Oncocin112, OhPrP-1 and 5 consistently decreased pyoverdine levels in both the PAO1-lasB::gfp and the clinical strain. However, an opposite phenomenon was seen for OhPrP-4 and OhPrP-2. Specifically, for MIC/2 treatments of OhPrP-2 and 4, high levels of pyoverdine were produced, accounting for lowest percent pyoverdine inhibitions recorded for the clinical isolate (Figure 18(b,d)). Finally, swarming motility was efficient at sub-inhibitory concentrations for Oncocin112, OhPrP-3 and 5 (Figure 19(a–c)). Halo diameters observed doubled with increasing incubation time, showing effective swarm response (Supporting Information Figures S9a to S10c). No visible growth was observed for their MICs.

Discussion

In this work, physical and chemical characteristics of the bioactive peptide of *O. hiatula* were evaluated. From solubility tests, RP-HPLC and AA composition analyses, the peptide extract is hydrophobic, acidic and relatively pure. The level of peptide purity observed from RP-HPLC chromatograms is attributable to the precipitation and elution procedure—the adsorption-desorption mechanism of peptides and proteins (Xindu & Regnier, 1984). Clearly, acetone precipitation from the acetic acid tissue hydrolysate did not only provide good yields of

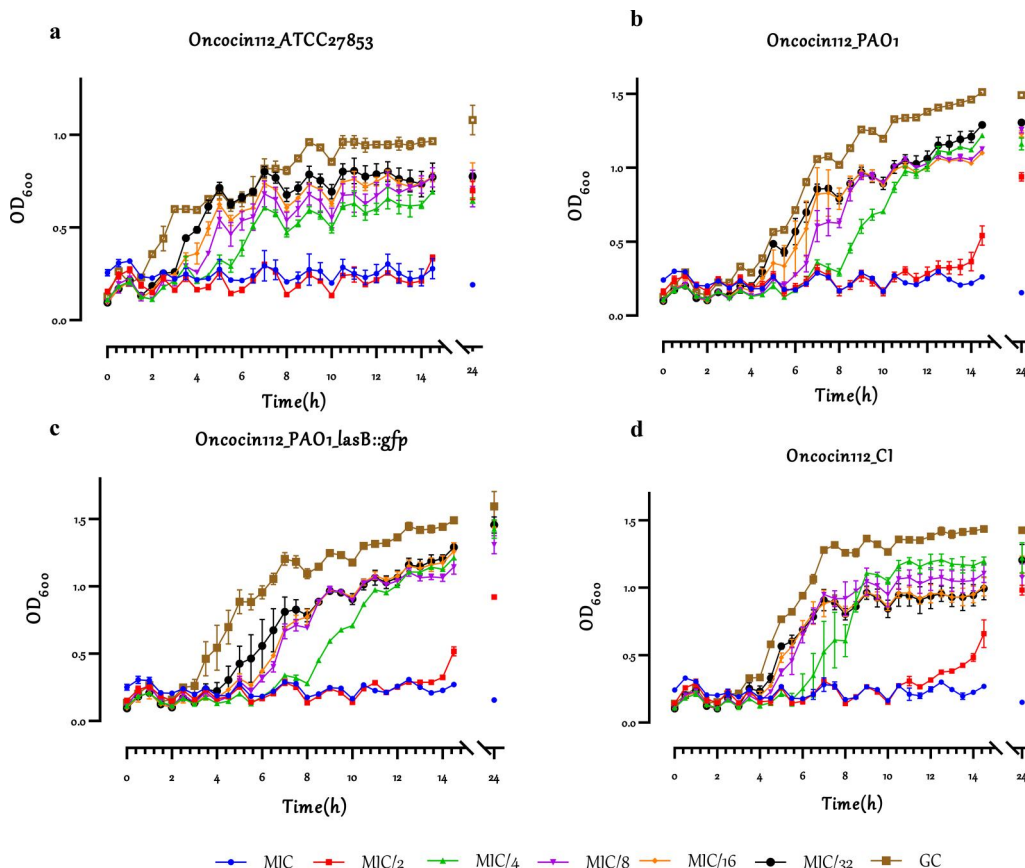


Figure 12. Bacteria growth inhibitory kinetics studied by increasing turbidity (OD600) with respect to time at different peptide concentrations; minimum inhibitory concentration (MIC) and sub-MICs, as well as the growth control (GC). Turbidimetric effects produced with Oncocin112 treatments of *Pseudomonas aeruginosa* (a) ATCC27853, (b) wild type PAO1, (c) PAO1-lasB::gfp (d) clinical isolate (CI).

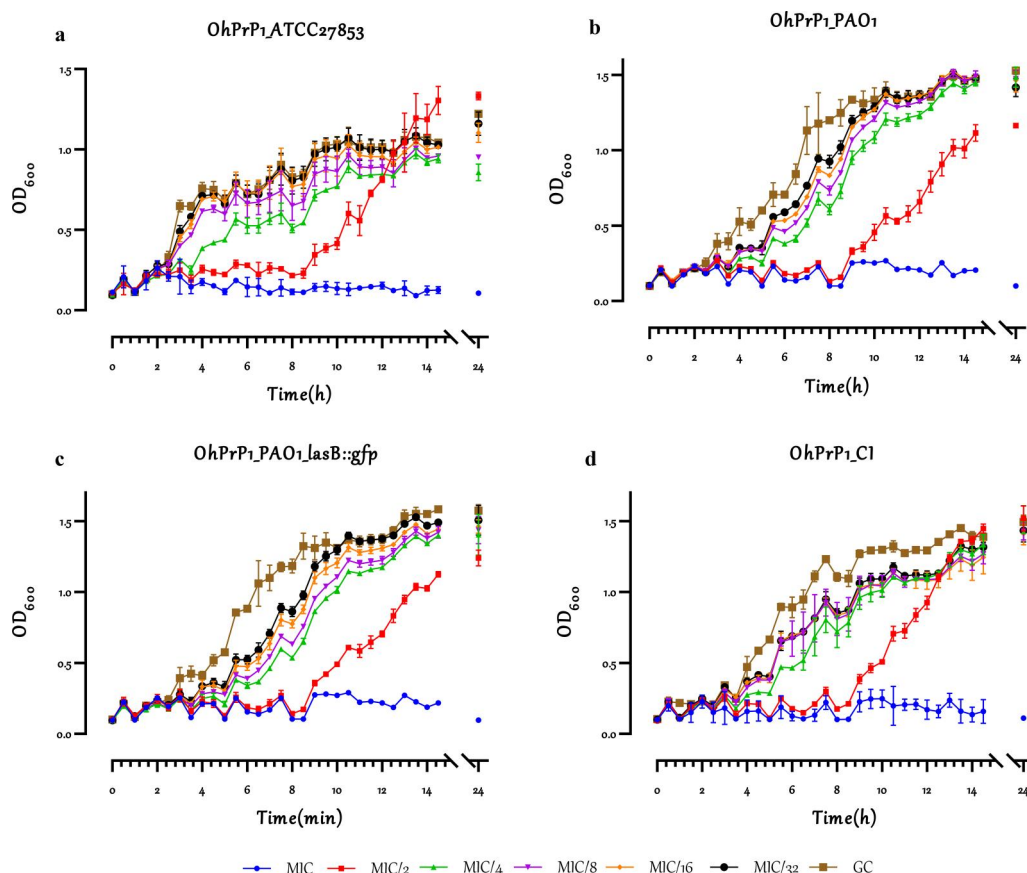


Figure 13. Turbidimetric effects produced with OhPrP-1 treatments of *Pseudomonas aeruginosa* (a) ATCC27853, (b) wild type PAO1, (c) PAO1-lasB::gfp (d) clinical isolate (CI). Changes in OD₆₀₀ at the minimum inhibitory concentration (MIC) and sub-MICs, as well as the growth control (GC) are plotted with respective colored dots and lines.

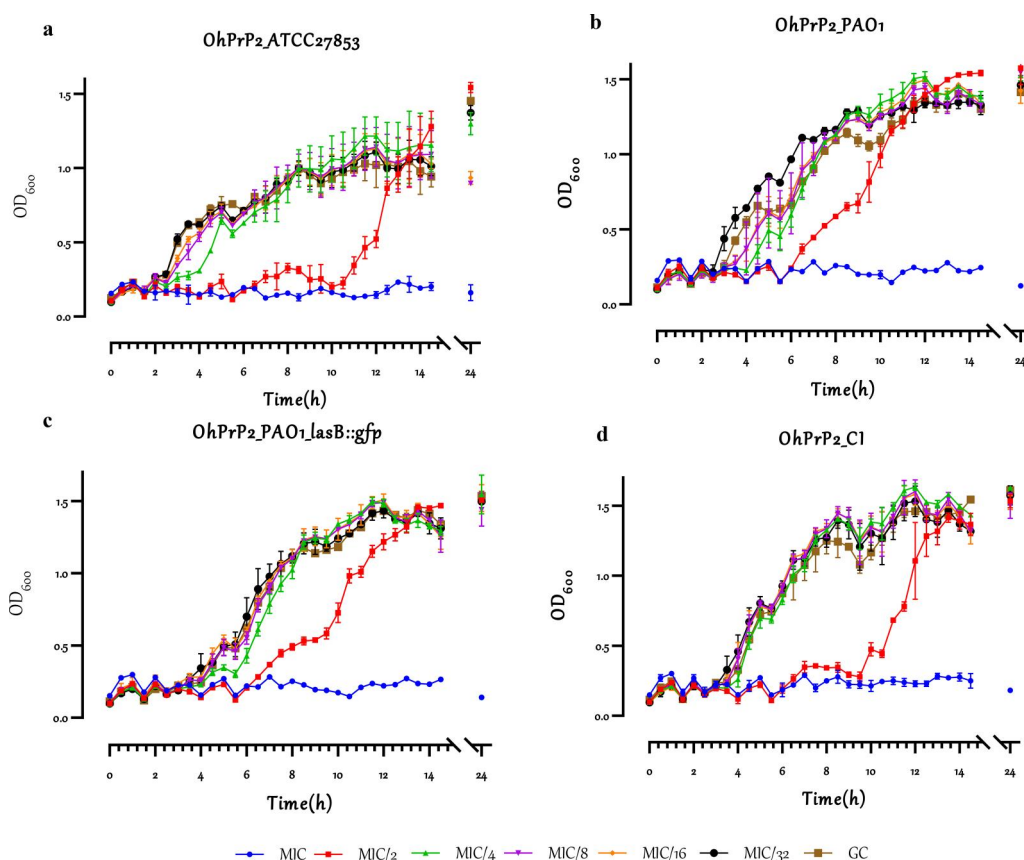


Figure 14. Bacteria growth inhibitory kinetics with OhPrP-2 treatments using *Pseudomonas aeruginosa* (a) ATCC27853, (b) wild type PAO1, (c) PAO1-lasB::gfp (d) clinical isolate (CI). Variations in OD₆₀₀ with respect to time at different peptide concentrations; minimum inhibitory concentration (MIC) and sub-MICs are shown in the plots.

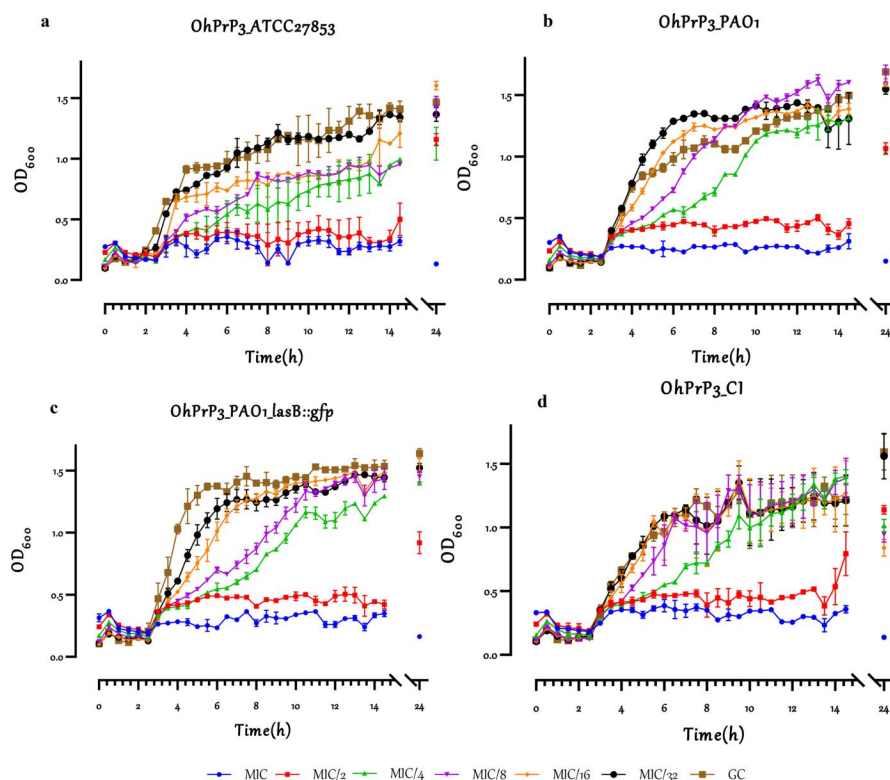


Figure 15. Growth inhibitory kinetics due to changes in absorbance (OD₆₀₀) with respect to time, at different OhPrP-3 treatments of *Pseudomonas aeruginosa* (a) ATCC27853, (b) wild type PAO1, (c) PAO1-lasB::gfp (d) clinical isolate (CI) cultures.

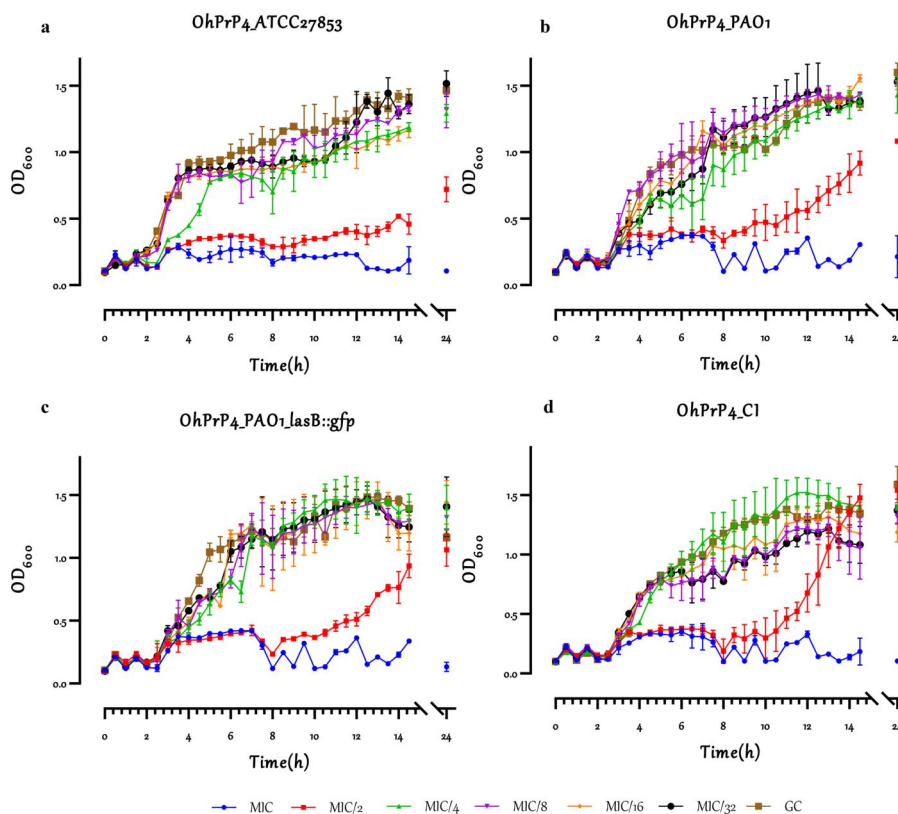


Figure 16. Turbidimetric effects produced with OhPrP-4 treatments of *Pseudomonas aeruginosa* (a) ATCC27853, (b) wild type PAO1, (c) PAO1-lasB::gfp (d) clinical isolate (CI) cultures. Bacteria growth inhibitory kinetics studied by increasing absorbance (OD₆₀₀) with respect to time at different peptide concentrations; minimum inhibitory concentration (MIC) and sub-MICs.

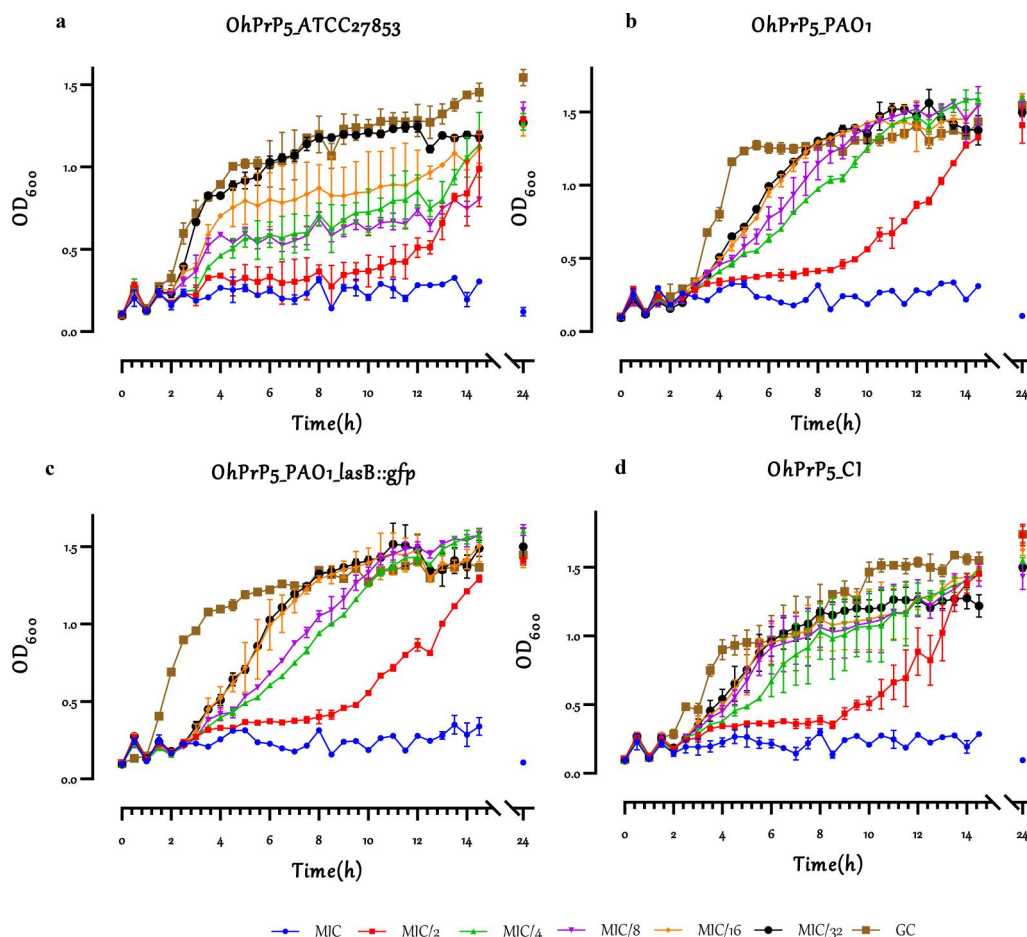


Figure 17. Turbidimetric plots showing changes in OD600 with respect to time as a result of OhPrP-5 treatments of *Pseudomonas aeruginosa* (a) ATCC27853, (b) wild type PAO1, (c) PAO1-lasB::gfp (d) clinical isolate (CI) cultures.

peptides with improved purity, but an added advantage of removal of lipids, non-ionic detergents, glycerol and salts (Novák & Havlíček, 2016; Ozols, 1990). Peptide purity by acetone precipitation has been observed in the work of Pedersen et al. in 1994 on metallothioneins. Pedersen et al. used a similar precipitation and purity analysis approach in their analysis of peptides from the midgut gland of a shore crab and observed two peaks in the chromatogram, being principally the same peptide (Pedersen et al., 1994).

UV-Vis analysis of the peptide absorptions revealed little aromatic AA content which was in agreement with results obtained from the AA quantitation. Maximum absorbance at 194 nm and the lower shoulder at 240 nm, are likely due to peptide backbone $\pi \rightarrow \pi^*$ transitions, and contributions from side chains of aspartic acid (Asp), glutamic acid (Glu), asparagine (Asn), glutamine (Gln), arginine (Arg) and histidine (His). The weakest absorption observed at 280 nm, is attributed to phenylalanine absorption. Similarly, Oncocin112 has tyrosine in its sequence, thus, extra UV-Vis absorptions were observed at 220 nm and 280 nm compared to the OhPrP-s. All AAs observed to be present in the peptide extract have been described to be characteristic of naturally occurring AMPs (Destoumieux-Garzón et al., 2016; Wang, 2019). Acidic properties of the peptide extract are due to the high glutamic and aspartic acid concentrations. The observed hydrophobicity of *O. hiatula* AMP can be related to high levels of

alanine, leucine, proline and hydroxyproline, among others. In addition, the presence of hydroxyproline could mean that *O. hiatula* AMP is concentrated in skin tissues (Kumar Srivastava et al., 2016), and perhaps released into its mucus for protection against infection.

Methionine, alanine, leucine, glutamate and uncharged lysine ('MALEK') found in the peptide, explains alpha-helical features observed in IR spectra reported previously (Gasu et al., 2018, 2019). Also, high glycine and proline in protein structures could lead to the formation of unordered conformations. Unordered peptides are usually unstable in solution due to flexibility of secondary structure, hence high aggregation propensity (Petkov et al., 2019). It has been shown both theoretically and experimentally that many AMPs are partly or fully disordered in solution but acquire a stable or defined structure at their functional sites (Petkov et al., 2019). It is possible that *O. hiatula* AMP falls in this category of unstable peptides because of its high hydrophobicity and high affinity for the HPLC column material. Second, peptides with high aggregation propensity in hydrophilic solutions such as buffers, display column retention behavior similar to what was observed for *O. hiatula* peptide (Lee et al., 2003). Accordingly, aggregation was anticipated as a potential bottleneck for *de novo* sequencing workflows. Attempts to obtain the primary structure (sequence) of the peptide by mass spectrometry failed primarily due to aggregation issues.

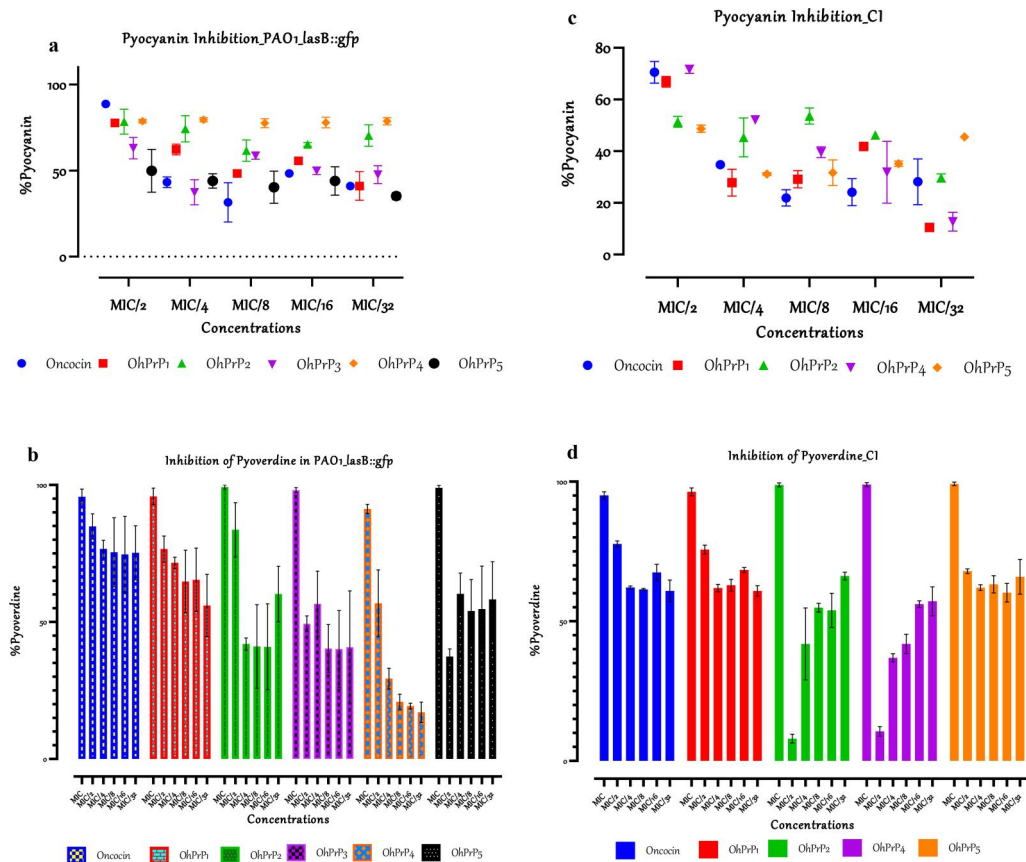


Figure 18. Extent of inhibition of siderophore expression; pyocyanin (a and c) and pyoverdine (b and d), in treated cultures of *Pseudomonas aeruginosa* PAO1-lasB::gfp strain and clinical isolate (CI).

Challenges such as sampling sources, extraction-isolation yield, undesirable chemophysical features like high hydrophobicity, aggregation or self-association and proteogenicity, impact negatively on isolation and characterization, and as a result, impede progress in the discovery and optimization of natural peptides from marine invertebrates (Dijksteel et al., 2021; Sperstad et al., 2011). With the growing need for novel antimicrobial agents to ease the burden of multidrug resistance, predicting novel candidate peptides from the sequences of naturally occurring counterparts have provided a complementary approach for AMP discovery and development (Cardoso et al., 2020; León-Buitimea et al., 2020). The use of computational tools has not only helped in prediction of AMPs with desirable chemophysical properties but has, in addition, provided insights for activity prediction and target elucidation. Due to the high percentage of proline in the bioactive peptide extract, designing AMPs from its AA composition meant that prediction algorithms and design strategies lead to the generation of peptide candidates that have essential PrAMP features—antimicrobial activity, binding to the 70S ribosome and/or DnaK.

PrAMPs mostly kill gram-negative bacteria by interfering with protein synthesis and enhancing protein misfolding by bacterial chaperone inhibition, with no known toxicities to mammalian erythrocytes (Gagnon et al., 2016; Graf et al., 2017; Mishra et al., 2018). Peptide design considerations yielded expected outcomes as OhPrP-5 aligned well with Metalnikowin and Api137 structurally, suggesting it could

bind and inhibit ribosomal function. Similarly, OhPrP-1, and 4 being structurally similar to ribonucleoproteins, OhPrP-2; ribosomal protein entity, as well as OhPrP-3; a spliceosomal protein segment, could inhibit protein synthesis and DNA replication. The DBAASP webserver was designed to predict membrane targeting AMPs. Comparing the physicochemical features of the designed peptides to LL-23 reveals membrane interaction propensity; however, due to comparatively high depths of penetration of the OhPrPs, direct translocation into bacterial cells to inhibit intracellular targets is also probable. Again, the penetration depth and tilt angle of OhPrP5 suggests its potential as a membrane targeting peptide. The physicochemical properties of known PrAMPs were thus matched to those of the designed peptides in order to guide peptide candidate selection. Most of the properties estimated for the designed peptides were similar when compared to those of Oncocin112 and Metalnikowin, fitting them in the same AMP class. Their cationic nature, estimated tilt angles, amphiphilicity, penetration depths and isoelectric points suggest, once again, that they could translocate across bacterial membranes to interact with intracellular targets such as the ribosome and nucleic acids. The properties of the OhPrP-s, having been obtained from the AA composition data and machine learning, corroborates the premise that *O. hiattula* peptide probably target nucleic acids and the ribosomes in bacteria.

Threading templates for OhPrP-s matching with ribonucleoproteins, spliceosomal proteins and PrAMPs, means that,

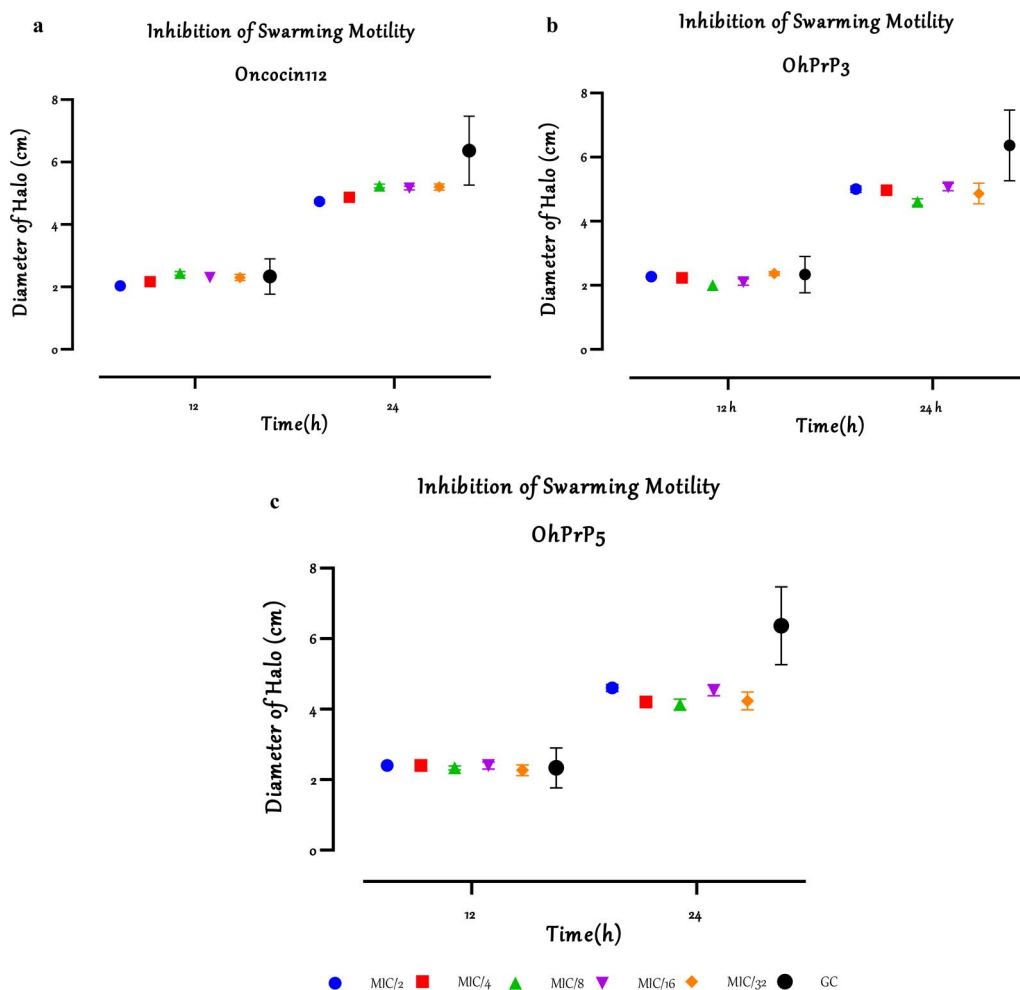


Figure 19. Extent of single colony swarming determined by halo diameter measurement after 12 and 24 h of incubation of treated (a: Oncocin112, b: OhPrP-3 and c: OhPrP-5) and untreated cultures of *Pseudomonas aeruginosa* PAO1-lasB::gfp strain.

the adopted design strategy resulted in the generation of putative peptides that could bind to the ribosome and nucleic acids as envisaged. All five peptides designed had very similar physicochemical property predictions, suggesting only little disparity in *in vitro* observations. Synthetic oligomers showing high water solubility *in vitro* during bacterial susceptibility testing, shows that database predictions such as low propensity to aggregate *in vitro*, were accurate. The work of Wang et al. for instance, incorporated input variable selection (AA and pseudo-AA composition which also incorporated electrostatic charge, codon diversity, molecular volume, polarity and secondary structure), to existing machine learning approaches in the design of an AMP prediction tool. On the basis that AAs play an important role in the antimicrobial activity of a peptide, this tool achieved high AMP discovery success rates (Van Oort et al., 2021; Wang et al., 2011). This observation correlated well with our observations.

Crystallographic data show that Oncocin112 blocks the peptidyl transferase center and destabilizes the initiation complex. Upon binding to the upper region of the peptide exit tunnel, Oncocin interferes with binding of the aminoacyl-tRNA (aa-tRNA) in the A-site. Although it allows formation of the initiation complex, the steric occlusion it causes destabilizes the initiation complex and causes dissociation. Like poking a screw driver into a computer—leading to loss

of function, Oncocin inhibits protein translation by preventing the transition from initiation to elongation (Kuriata et al., 2019). Molecular docking of the full length Oncocin112 and co-crystallized Oncocin112, as well as the OhPrP-s to the 50S subunit of the ribosome and DnaK produced binding conformations within the processing site of the ribosome and the substrate binding site of DnaK. Docked peptide conformers deviated slightly from their experimental counterparts due to structural flexibility in most cases, hence the recorded RMSD values. Docking of the 13-mer gave high binding affinity for the ribosome compared to DnaK. OhPrP-3 and 5 binding within similar binding sites in the ribosome and DnaK, suggests similar interactions and modes of action. A good overlap of OhPrP-1 and 4 within a similar site could suggest a similar selectivity, though their binding affinities were not estimated, just as the 19-mer Oncocin112. OhPrP-2 binding towards the exit tunnel was unique, which confirms deviation expected for a negative control. This means that, OhPrP-1, 3, 4 and 5 are capable of antibacterial activity similar to Oncocin112 and its related PrAMPs, Metalnikowin and Api137. Moreover, this could mean that the docking protocol employed to determine both binding affinities and poses are valid.

The identification of the 70S ribosome as primary target and consecutive studies providing the structures of

Oncocin112- and Api137-ribosome complexes allow quantifying the PrAMP-ribosome binding for different bacteria to explore their maximal activity spectrum. This approach neglects culture medium compositions, which strongly affect the MIC values, as well as the cellular uptake (Kolano et al., 2020). On the contrary, here-in, peptide-target interactions were evaluated *in silico*. And the use of the unique pharmacodynamic parameter, MIC, for the description peptide potency was complemented with the determination of a bactericidal concentration and the study of time course growth inhibition. Peptides with *in silico* binding modes similar to Oncocin112, produced similar *in vitro* results. For example, OhPrP-3 and 5 binding to the ribosome and DnaK, at similar positions as Oncocin112 (and Metalnikowin), produced the same *in vitro* bactericidal effects. The same was found for OhPrP-1 and 4. Conversely, OhPrP-2 was predicted to bind particularly at the exit tunnel (a single ribosomal functional site) with relatively a small number of nonbonding interactions, hence, probably responsible for its bacteriostatic effect.

In *E. coli*, proline-rich AMPs depend on the membrane transporter protein SbmA for full activity. Conversely, species deficient of SbmA, such as *P. aeruginosa*, are less susceptible to this class of AMPs (Frimodt-Møller et al., 2022). This explains why Gram-positive bacteria, in general, are resistant to proline-rich AMPs. This could also explain the similarities of the MIC values of OhPrPs against different *P. aeruginosa* strains used in this work. Bactericidal activities recorded at the MIC could mean that, the peptides have to bind to inhibit the ribosome as the main target, and at the same time, DnaK as one of many off targets. Hence, ribosome and DnaK binding could be the ultimate mechanism for the bactericidal activities of OhPrP-1, 3, 4 and 5.

Swarming motility at MICs was abolished due to bactericidal effects of Oncocin112, OhPrP-3 and 5. Oncocin112, OhPrP-3 and OhPrP-5 binding to LasR *in silico* correlate to reduction of pyocyanin and pyoverdine levels. From the observed antivirulence activity, it can be postulated that peptide-LasR binding modes could permit peptides to interact directly with LasR regulated genes, thereby interfering with LasR quorum sensing activation (Fan et al., 2013). The dnaK gene of *P. aeruginosa* has been associated with bacterial motility (Okuda et al., 2017), but since a dose-dependent inhibition of swarming motility was not observed for the peptides at sub-MIC concentrations, we cannot directly associate DnaK-peptide binding to inhibition of swarming motility.

Conclusion

Acetone precipitation of AMPs from *O. hiatula* body tissue hydrolysate yielded pure peptides with high proline and acidic AAs content. Cellular targets for bioactive peptides with such AA signatures are the ribosome and nucleic acids. This work is limited by the absence of sequence information on the natural peptide extracted. However, computer-aided design yielded five novel AMPs with very good physicochemical properties. Molecular modelling confirmed structural

semblance of OhPrP-s to ribosome and nucleic acid binding peptides. The peptides designed had both bactericidal and antivirulent potential *in vitro*. *In silico* and *in vitro* evidence support the premise that, the AMP from *O. hiatula* could bind multiple intracellular targets, namely the ribosome and nucleic acids, for its antibacterial activities. Taken together, this work demonstrates an approach of merging biophysical characterization and knowledge-based peptide design strategies, to overturn challenges of marine peptide discovery and help with the discovery of new bioactive AMPs with known targets.

Acknowledgements

The authors are grateful to Prof. Scott Rice of Nanyang Technological University, Singapore for the kind donations of the *P. aeruginosa* PA01 and lasB-gfp strains. Mr. William Ofori Appaw of the Mycotoxin Lab of KNUST is also acknowledged for providing generous access to his HPLC during this study.

Disclosure statement

All authors declare that there were no financial, professional or personal competing interests that might have influenced the performance or presentation of this study.

Funding

This study was funded, in part, by the Ideas Matter Doctoral Fellowship awarded by the West African Research Association in collaboration with the Mastercard Foundation in 2020 to ENG.

ORCID

Edward Ntim Gasu  <http://orcid.org/0000-0002-1752-0948>

Lawrence Sheringham Borquaye  <http://orcid.org/0000-0002-5037-0777>

Authors' contributions

LSB and ENG conceived the study. All experiments were designed by LSB, JKM and ENG. All experiments were carried out by ENG. Data analyses were by ENG, JKM and LSB. Work was supervised by LSB and JKM. Manuscript was prepared by ENG and reviewed by JKM and LSB. All authors read and approved the final manuscript.

Data availability statement

All data generated or analyzed during this study are included in this published article.

References

- Adonizio, A., Kong, K. F., & Mathee, K. (2008). Inhibition of quorum sensing-controlled virulence factor production in *Pseudomonas aeruginosa* by South Florida plant extracts. *Antimicrobial Agents and Chemotherapy*, 52(1), 198–203. <https://doi.org/10.1128/AAC.00612-07>
- Altschul, S. F., Madden, T. L., Schäffer, A. A., Zhang, J., Zhang, Z., Miller, W., & Lipman, D. J. (1997). Gapped BLAST and PSI-BLAST: A new generation of protein database search programs. *Nucleic Acids Research*, 25(17), 3389–3402. <https://doi.org/10.1093/nar/25.17.3389>
- Antunes, D. A., Moll, M., Devaurs, D., Jackson, K., Liz, G., & Kavraki, L. E. (2017). DINC 2.0: A new protein-peptide docking webserver using an

- incremental approach. *Cancer Research*, 77(21), e55–e57. <https://doi.org/10.1158/0008-5472.CAN-17-0511>
- Batoni, G., Maisetta, G., & Esin, S. (2016). Antimicrobial peptides and their interaction with biofilms of medically relevant bacteria. *Biochimica et Biophysica Acta*, 1858(5), 1044–1060. <https://doi.org/10.1016/j.bbame.2015.10.013>
- Beyer, P., & Paulin, S. (2020). The antibacterial research and development pipeline needs urgent solutions. *ACS Infectious Diseases*, 6(6), 1289–1291. <https://doi.org/10.1021/acscinfecdis.0c00044>
- Borquaye, L. S., Darko, G., Ocansey, E., & Ankomah, E. (2015). Antimicrobial and antioxidant properties of the crude peptide extracts of *Galatea paradoxa* and *Patella rustica*. *SpringerPlus*, 4(1), 500. <https://doi.org/10.1186/s40064-015-1266-2>
- Borquaye, L. S., Darko, G., Laryea, M. K., Roberts, V., Boateng, R., & Gasu, E. N. (2017). Anti-inflammatory activities of extracts from *Oliva* Sp., *Patella rustica*, and *Littorina littorea* collected from Ghana's coastal shorelines. *Cogent Biology*, 3(1), 1364063. <https://doi.org/10.1080/23312025.2017.1364063>
- Borquaye, L. S., Darko, G., Oklu, N., Anson-Yevu, C., & Ababio, A. (2016). Antimicrobial and antioxidant activities of ethyl acetate and methanol extracts of *Littorina littorea* and *Galatea paradoxa*. *Cogent Chemistry*, 2(1), 1161865. <https://doi.org/10.1080/23312009.2016.1161865>
- Campbell, J. (2011). High-throughput assessment of bacterial growth inhibition by optical density measurements. *Current Protocols in Chemical Biology*, 3(3), 1–20.
- Cardoso, M. H., Orozco, R. Q., Rezende, S. B., Rodrigues, G., Oshiro, K. G. N., & Cândido, E. S. (2020). Computer-aided design of antimicrobial peptides: Are we generating effective drug candidates? *Frontiers in Immunology*, 10(January), 1–15.
- Cruz, V. L., Ramos, J., Martinez-salazar, J., Montalban-lopez, M., & Maqueda, M. (2021). The role of key amino acids in the antimicrobial mechanism of a bacteriocin model revealed by molecular simulations. *Journal of Chemical Information and Modeling*, 61(12), 6066–6078. <https://doi.org/10.1021/acs.jcim.1c00838>
- Das, M. C., Sandhu, P., Gupta, P., Rudrapaul, P., De, U. C., Tribedi, P., Akhter, Y., & Bhattacharjee, S. (2016). Attenuation of *Pseudomonas aeruginosa* biofilm formation by Vitexin: A combinatorial study with azithromycin and gentamicin. *Scientific Reports*, 6, 23347–23313. <https://doi.org/10.1038/srep23347>
- Destoumieux-Garzon, D., Rosa, R. D., Schmitt, P., Barreto, C., Vidal-Dupiol, J., Mitta, G., Gueguen, Y., & Bachère, E. (2016). Antimicrobial peptides in marine invertebrate health and disease. *Philosophical Transactions of the Royal Society B: Biological Sciences*, 371(1695), 20150300. <https://doi.org/10.1098/rstb.2015.0300>
- Dijksteel, G. S., Ulrich, M. M. W., Middelkoop, E., & Boekema, B. K. H. L. (2021). Lessons learned from clinical trials using antimicrobial peptides (AMPs). *Frontiers in Microbiology*, 12(February), 616979–616918. <https://doi.org/10.3389/fmicb.2021.616979>
- Fan, H., Dong, Y., Wu, D., Bowler, M. W., Zhang, L., & Song, H. (2013). QsIA disrupts LasR dimerization in anti-inactivation of bacterial quorum sensing. *Proceedings of the National Academy of Sciences of the United States of America*, 110(51), 20765–20770. <https://doi.org/10.1073/pnas.1314415110>
- Fedders, H., & Leippe, M. (2008). A reverse search for antimicrobial peptides in *Ciona intestinalis*: Identification of a gene family expressed in hemocytes and evaluation of activity. *Developmental and Comparative Immunology*, 32(3), 286–298. <https://doi.org/10.1016/j.dci.2007.06.003>
- Fedders, H., Michalek, M., Grötzinger, J., & Leippe, M. (2008). An exceptional salt-tolerant antimicrobial peptide derived from a novel gene family of haemocytes of the marine invertebrate *Ciona intestinalis*. *The Biochemical Journal*, 416(1), 65–75. <https://doi.org/10.1042/BJ20080398>
- Fedders, H., Podschun, R., & Leippe, M. (2010). The antimicrobial peptide Ci-MAM-A24 is highly active against multidrug-resistant and anaerobic bacteria pathogenic for humans. *International Journal of Antimicrobial Agents*, 36(3), 264–266. <https://doi.org/10.1016/j.ijantimicag.2010.04.008>
- Frimodt-Møller, J., Campion, C., Nielsen, P. E., & Løbner-Olesen, A. (2022). Translocation of non-lytic antimicrobial peptides and bacteria penetrating peptides across the inner membrane of the bacterial envelope. *Current Genetics*, 68(1), 83–90. <https://doi.org/10.1007/s00294-021-01217-9>
- Gagnon, M. G., Roy, R. N., Lomakin, I. B., Florin, T., Mankin, A. S., & Steitz, T. A. (2016). Structures of proline-rich peptides bound to the ribosome reveal a common mechanism of protein synthesis inhibition. *Nucleic Acids Research*, 44(5), 2439–2450. <https://doi.org/10.1093/nar/gkw018>
- Ganz, T. (2003). The role of antimicrobial peptides in innate immunity. *Integrative and Comparative Biology*, 43(2), 300–304. <https://doi.org/10.1093/icb/43.2.300>
- Gasu, E. N., Ahor, H. S., & Borquaye, L. S. (2018). Peptide extract from *Olivancillaria hiatala* exhibits broad-spectrum antibacterial activity. *BioMed Research International*, 2018, 6010572–6010511. (Article ID 6010572):<https://doi.org/10.1155/2018/6010572>
- Gasu, E. N., Ahor, H. S., & Borquaye, L. S. (2019). Peptide mix from *Olivancillaria hiatala* interferes with cell-to-cell communication in *Pseudomonas aeruginosa*. *BioMed Research International*, 2019, 5313918–5313912 (Article ID 5313918). <https://doi.org/10.1155/2019/5313918>
- Genevaux, P., Keppel, F., Schwager, F., Langendijk-Genevaux, P. S., Hartl, F. U., & Georgopoulos, C. (2004). In vivo analysis of the overlapping functions of DnaK and trigger factor. *EMBO Reports*, 5(2), 195–200. <https://doi.org/10.1038/sj.embor.7400067>
- Graf, M., Mardirossian, M., Nguyen, F., Seefeldt, A. C., Guichard, G., Scocchi, M., Innis, C. A., & Wilson, D. N. (2017). Proline-rich antimicrobial peptides targeting protein synthesis. *Natural Product Reports*, 34(7), 702–711. <https://doi.org/10.1039/c7np00020k>
- Herbert, P., Barros, P., Ratola, N., & Alves, A. (2000). HPLC determination of amino acids in musts and port wine using OPA/FMOC derivatives. *Journal of Food Science*, 65(7), 1130–1133. <https://doi.org/10.1111/j.1365-2621.2000.tb10251.x>
- Huan, Y., Kong, Q., Mou, H., & Yi, H. (2020). Antimicrobial peptides: Classification, design, application and research progress in multiple fields. *Frontiers in Microbiology*, 11, 1–21. <https://doi.org/10.3389/fmicb.2020.582779>
- Inoue, T., Shingaki, R., & Fukui, K. (2008). Inhibition of swarming motility of *Pseudomonas aeruginosa* by branched-chain fatty acids. *FEMS Microbiology Letters*, 281(1), 81–86. <https://doi.org/10.1111/j.1574-6968.2008.01089.x>
- Jang, W. S., Kim, K. N., Lee, Y. S., Nam, M. H., & Lee, I. H. (2002). Halocidin: A new antimicrobial peptide from hemocytes of the solitary tunicate, *Halocynthia aurantium*. *FEBS Letters*, 521(1–3), 81–86. [https://doi.org/10.1016/S0014-5793\(02\)02827-2](https://doi.org/10.1016/S0014-5793(02)02827-2)
- Jonas, K., Liu, J., Chien, P., & Laub, M. T. (2013). Proteotoxic stress induces a cell-cycle arrest by stimulating lon to degrade the replication initiator DnaA. *Cell*, 154(3), 623–636. <https://doi.org/10.1016/j.cell.2013.06.034>
- Knappe, D., Zahn, M., Sauer, U., Schiffer, G., Sträter, N., & Hoffmann, R. (2011). Rational design of oncocin derivatives with superior protease stabilities and antibacterial activities based on the high-resolution structure of the Oncocin-DnaK complex. *ChemBiochem: A European Journal of Chemical Biology*, 12(6), 874–876. <https://doi.org/10.1002/cbic.201000792>
- Köhler, T., Dumas, J. L., & Van Delden, C. (2007). Ribosome protection prevents azithromycin-mediated quorum-sensing modulation and stationary-phase killing of *Pseudomonas aeruginosa*. *Antimicrobial Agents and Chemotherapy*, 51(12), 4243–4248. <https://doi.org/10.1128/AAC.00613-07>
- Kolano, L., Knappe, D., Volke, D., Sträter, N., & Hoffmann, R. (2020). Ribosomal target-binding sites of antimicrobial peptides Api137 and Onc112 are conserved among pathogens indicating new lead structures to develop novel broad-spectrum antibiotics. *ChemBiochem: A European Journal of Chemical Biology*, 21(18), 2628–2634. <https://doi.org/10.1002/cbic.202000109>
- Kostylev, M., Kim, D. Y., Smalley, N. E., Salukhe, I., Greenberg, E. P., & Dandekar, A. A. (2019). Evolution of the *Pseudomonas aeruginosa* quorum-sensing hierarchy. *Proceedings of the National Academy of Sciences of the United States of America*, 116(14), 7027–7032. <https://doi.org/10.1073/pnas.1819796116>

- Kumar Srivastava, A., Khare, P., Kumar Nagar, H., Raghuwanshi, N., & Srivastava, R. (2016). Hydroxyproline: A potential biochemical marker and its role in the pathogenesis of different diseases. *Current Protein & Peptide Science*, 17(6), 596–602. <https://doi.org/10.2174/1389203717666151201192247>
- Kuriata, A., Iglesias, V., Pujols, J., Kurcinski, M., Kmiecik, S., & Ventura, S. (2019). Aggrescan3D (A3D) 2.0: Prediction and engineering of protein solubility. *Nucleic Acids Research*, 47(W1), W300–W307. <https://doi.org/10.1093/nar/gkz321>
- Lee, D. L., Mant, C. T., & Hodges, R. S. (2003). A novel method to measure self-association of small amphipathic molecules ; temperature profiling in reversed-phase chromatography. *Journal of Biological Chemistry*, 278(25), 22918–22927. <https://doi.org/10.1074/jbc.M301777200>
- Lee, I. H., Lee, Y. S., Kim, C. H., Kim, C. R., Hong, T., Menzel, L., Boo, L. M., Pohl, J., Sherman, M. A., Waring, A., & Lehrer, R. I. (2001). Dicythaurin: An antimicrobial peptide from hemocytes of the solitary tunicate, *Halocynthia aurantium*. *Biochimica et Biophysica Acta (BBA)—General Subjects*, 1527(3), 141–148. [https://doi.org/10.1016/S0304-4165\(01\)00156-8](https://doi.org/10.1016/S0304-4165(01)00156-8)
- León-Buitimea, A., Garza-cárdenas, C. R., Garza-cervantes, J. A., Lerma-Escalera, J. A., & Morones-Ramírez, J. R. (2020). The demand for new antibiotics : Antimicrobial peptides, therapies as future strategies in antibacterial agent design. *Frontiers in Microbiology*, 21, 1–10. (July): <https://doi.org/10.3389/fmicb.2020.01669>
- Li, C., Haug, T., Moe, M. K., Styrvold, O. B., & Stensvåg, K. (2010). Centrocins: Isolation and characterization of novel dimeric antimicrobial peptides from the green sea urchin, *Strongylocentrotus droebachiensis*. *Developmental and Comparative Immunology*, 34(9), 959–968. <https://doi.org/10.1016/j.dci.2010.04.004>
- Mant, C. T., Jiang, Z., Gera, L., Davis, T., Nelson, K. L., Bevers, S., & Hodges, R. S. (2019). De novo designed amphipathic α - helical antimicrobial peptides incorporating dab and dap residues on the polar face to treat the gram-negative pathogen, *Acinetobacter baumannii*. *Journal of Medicinal Chemistry*, 62(7), 3354–3366. <https://doi.org/10.1021/acs.jmedchem.8b01785>
- Matos de Opitz, C. L., & Sass, P. (2020). Tackling antimicrobial resistance by exploring new mechanisms of antibiotic action. *Future Microbiology*, 15(9), 703–708. <https://doi.org/10.2217/fmb-2020-0048>
- Mishra, A. K., Choi, J., Moon, E., & Baek, K. H. (2018). Tryptophan-rich and proline-rich antimicrobial peptides. *Molecules*, 23(4), 815–823. <https://doi.org/10.3390/molecules23040815>
- Mishra, B., & Wang, G. (2012). The importance of amino acid composition in natural AMPs : An evolutionary, structural, and functional perspective. *Frontiers in Immunology*, 3(July), 221–223. <https://doi.org/10.3389/fimmu.2012.00221>
- Musthafa, K. S., Sivamaruthi, B. S., Pandian, S. K., & Ravi, A. V. (2012). Quorum sensing inhibition in *Pseudomonas aeruginosa* PAO1 by antagonistic compound phenylacetic acid. *Current Microbiology*, 65(5), 475–480. <https://doi.org/10.1007/s00284-012-0181-9>
- Novák, P., & Havlíček, V. (2016). Protein extraction and precipitation. In *Proteomic profiling and analytical chemistry: The crossroads* (2nd ed., Elsevier, pp. 52–62).
- Ohtsuka, Y., & Inagaki, H. (2020). In silico identification and functional validation of linear cationic α -helical antimicrobial peptides in the ascidian *Ciona intestinalis*. *Scientific Reports*, 10(1), 1–9. <https://doi.org/10.1038/s41598-020-69485-y>
- Okuda, J., Yamane, S., Nagata, S., Kunikata, C., Suezawa, C., & Yasuda, M. (2017). The *Pseudomonas aeruginosa* dnaK gene is involved in bacterial translocation across the intestinal epithelial cell barrier. *Microbiology (Reading, England)*, 163(8), 1208–1216. <https://doi.org/10.1099/mic.0.000508>
- Ozols, J. (1990). Amino acid analysis. *Methods in Enzymology*, 182(44), 587–601. [https://doi.org/10.1016/0076-6879\(90\)82046-5](https://doi.org/10.1016/0076-6879(90)82046-5)
- Pandit, G., Chowdhury, N., Mohid, A., Bidkar, A. P., Bhunia, A., & Chatterjee, S. (2021). Effect of secondary structure and side chain length of hydrophobic amino acid residues on the antimicrobial activity and toxicity of 14 residue long de novo AMPs. *ChemMedChem*, 16(2), 355–367. <https://doi.org/10.1002/cmdc.202000550>
- Pedersen, K. L., Pedersen, S. N., Højrup, P., Andersen, J. S., Roepstorff, P., Knudsen, J., & Depledge, M. H. (1994). Purification and characterization of a cadmium-induced metallothionein from the shore crab *Carcinus maenas* (L.). *Biochemical Journal*, 297(3), 609–614. <https://doi.org/10.1042/bj2970609>
- Petkov, P., Lilkova, E., Ilieva, N., & Litov, L. (2019). Self-association of antimicrobial peptides: A molecular dynamics simulation study on bombinin. *International Journal of Molecular Sciences*, 20(21), 5450–5423. <https://doi.org/10.3390/ijms20215450>
- Pettersen, E. F., Goddard, T. D., Huang, C. C., Couch, G. S., Greenblatt, D. M., Meng, E. C., & Ferrin, T. E. (2004). UCSF Chimera—A visualization system for exploratory research and analysis. *Journal of Computational Chemistry*, 25(13), 1605–1612. <https://doi.org/10.1002/jcc.20084>
- Pirtskhalava, M., Gabrielian, A., Cruz, P., Griggs, H. L., Squires, B., & Hurt, D. E. (2016). DBAASP v. 2 : An enhanced database of structure and antimicrobial/cytotoxic activity of natural and synthetic peptides. *Nucleic Acid Research*, 44(11), 1104–1112.
- Pletzer, D., & Hancock, R. E. W. (2016). Antibiofilm peptides: Potential as broadspectrum agents. *Journal of Bacteriology*, 198(19), 2572–2578. <https://doi.org/10.1128/JB.00017-16>
- Poehlsgaard, J., & Douthwaite, S. (2005). The bacterial ribosome as a target for antibiotics. *Nature Reviews. Microbiology*, 3(11), 870–881. <https://doi.org/10.1038/nrmicro1265>
- Rončević, T., Puizina, J., & Tossi, A. (2019). Antimicrobial peptides as anti-infective agents in pre-post-antibiotic era ? *International Journal of Molecular Sciences*, 20(22), 5713–5732. <https://doi.org/10.3390/ijms20225713>
- Roy, R. N., Lomakin, I. B., Gagnon, M. G., & Steitz, T. A. (2015). The mechanism of inhibition of protein synthesis by the proline-rich peptide oncocin. *Nature Structural & Molecular Biology*, 22(6), 466–469. <https://doi.org/10.1038/nsmb.3031>
- Schäffer, A. A., Aravind, L., Madden, T. L., Shavirin, S., Spouge, J. L., Wolf, Y. I., Koonin, E. V., & Altschul, S. F. (2001). Improving the accuracy of PSI-BLAST protein database searches with composition-based statistics and other refinements. *Nucleic Acids Research*, 29(14), 2994–3005.
- Schuster, R. (1988). Determination of amino acids in biological, pharmaceutical, plant and food samples by automated precolumn derivatization and high-performance liquid chromatography. *Journal of Chromatography B: Biomedical Sciences and Applications*, 431(C), 271–284. [https://doi.org/10.1016/S0378-4347\(00\)83096-0](https://doi.org/10.1016/S0378-4347(00)83096-0)
- Scopes, R. K. (1974). Measurement of protein by spectrophotometry at 205 nm. *Analytical Biochemistry*, 59(1), 277–282. [https://doi.org/10.1016/0003-2697\(74\)90034-7](https://doi.org/10.1016/0003-2697(74)90034-7)
- Seefeldt, A. C., Nguyen, F., Antunes, S., Pérébaskine, N., Graf, M., Arenz, S., Inampudi, K. K., Douat, C., Guichard, G., Wilson, D. N., & Innis, C. A. (2015). The proline-rich antimicrobial peptide Onc112 inhibits translation by blocking and destabilizing the initiation complex. *Nature Structural & Molecular Biology*, 22(6), 470–475. <https://doi.org/10.1038/nsmb.3034>
- Shah, M., Taylor, V. L., Bona, D., Tsao, Y., Stanley, S. Y., Pimentel-Elardo, S. M., McCallum, M., Bondy-Denomy, J., Howell, P. L., Nodwell, J. R., Davidson, A. R., Moraes, T. F., & Maxwell, K. L. (2021). A phage-encoded anti-activator inhibits quorum sensing in *Pseudomonas aeruginosa*. *Molecular Cell*, 81(3), 571–583.e6. <https://doi.org/10.1016/j.molcel.2020.12.011>
- Sperstad, S. V., Haug, T., Blencke, H. M., Styrvold, O. B., Li, C., & Stensvåg, K. (2011). Antimicrobial peptides from marine invertebrates : Challenges and perspectives in marine antimicrobial peptide discovery. *Biotechnology Advances*, 29(5), 519–530. <https://doi.org/10.1016/j.biotechadv.2011.05.021>
- Stothard, P. (2000). The sequence manipulation suite: JavaScript programs for analyzing and formatting protein and DNA sequences. *BioTechniques*, 28(6), 1102–1104. <https://doi.org/10.2144/00286ir01>
- Van Oort, C. M., Ferrell, J. B., Remington, J. M., Wshah, S., & Li, J. (2021). AMPGAN v2: Machine learning-guided design of antimicrobial peptides. *Journal of Chemical Information and Modeling*, 61(5), 2198–2207. <https://doi.org/10.1021/acs.jcim.0c01441>

- Vijayakumar, P. P., & Muriana, P. M. (2015). A microplate growth inhibition assay for screening bacteriocins against *Listeria monocytogenes* to differentiate their mode-of-action. *Biomolecules*, 5(2), 1178–1194. <https://doi.org/10.3390/biom5021178>
- Waghu, F. H., Barai, R. S., Gurung, P., & Idicula-thomas, S. (2016). CAMP R3: A database on sequences, structures and signatures of antimicrobial peptides. *Nucleic Acids Research*, 44(D1), D1094–D1097. <https://doi.org/10.1093/nar/gkv1051>
- Wang, G. (2019). The antimicrobial peptide database provides a platform for decoding the design principles of naturally occurring antimicrobial peptides. *Protein Science*, 29(1), 1–11.
- Wang, G., Elliott, M., Cogen, A. L., Ezell, E. L., Gallo, R. L., & Hancock, R. E. (2012). Structure, dynamics, and antimicrobial and immune modulatory activities of human LL-23 and its single-residue variants mutated on the basis of homologous primate cathelicidins. *Biochemistry*, 51(2), 653–664. <https://doi.org/10.1021/bi2016266>
- Wang, P., Hu, L., Liu, G., Jiang, N., Chen, X., Xu, J., Zheng, W., Li, L., Tan, M., Chen, Z., Song, H., Cai, Y.-D., & Chou, K.-C. (2011). Prediction of antimicrobial peptides based on sequence alignment and feature selection methods. *PLoS One*, 6(4), e18476–9. <https://doi.org/10.1371/journal.pone.0018476>
- Wiegand, I., Hilpert, K., & Hancock, R. (2008). Agar and broth dilution methods to determine the minimal inhibitory concentration (MIC) of antimicrobial substances. *Nature Protocols*, 3(2), 163–175. <https://doi.org/10.1038/nprot.2007.521>
- Wilson, D. N., Hauryliuk, V., Atkinson, G. C., & O'Neill, A. J. (2020). Target protection as a key antibiotic resistance mechanism. *Nature Reviews. Microbiology*, 18(11), 637–648. <https://doi.org/10.1038/s41579-020-0386-z>
- Xindu, G., & Regnier, F. E. (1984). Retention model for proteins in reversed-phase liquid chromatography. *Journal of Chromatography A*, 296(C), 15–30. [https://doi.org/10.1016/S0021-9673\(01\)96399-X](https://doi.org/10.1016/S0021-9673(01)96399-X)
- Yan, Y., Tao, H., He, J., & Huang, S. (2020). you. The HDock server for integrated protein–protein docking. *Nature Protocols*, 15(5), 1829–1852. <https://doi.org/10.1038/s41596-020-0312-x>
- Yang, J., & Zhang, Y. (2015). I-TASSER server : New development for protein structure and function predictions. *Nucleic Acids Research*, 43(W1), W174–W181. <https://doi.org/10.1093/nar/gkv342>